SMC-TR-05-16

AEROSPACE REPORT NO.
TR-2005(8555)-3

Image Analysis Study of the Porosity Characteristics of Nickel Sinter

15 April 2005

Prepared by

A. H. ZIMMERMAN and G. A. TO
Electronics and Photonics Laboratory
Laboratory Operations

Prepared for

SPACE AND MISSILE SYSTEMS CENTER
AIR FORCE SPACE COMMAND
2430 E. El Segundo Boulevard
Los Angeles Air Force Base, CA 90245

Engineering and Technology Group

THE AEROSPACE CORPORATION
El Segundo, California

This report was submitted by The Aerospace Corporation, El Segundo, CA 90245-4691, under Contract No. FA8802-04-C-0001 with the Space and Missile Systems Center, 2430 E. El Segundo Blvd., Los Angeles Air Force Base, CA 90245. It was reviewed and approved for The Aerospace Corporation by B. Jaduszliwer, Principal Director, Electronics and Photonics Laboratory. Michael Zambrana was the project officer for the Mission-Oriented Investigation and Experimentation (MOIE) program.

This report has been reviewed by the Public Affairs Office (PAS) and is releasable to the National Technical Information Service (NTIS). At NTIS, it will be available to the general public, including foreign nationals.

This technical report has been reviewed and is approved for publication. Publication of this report does not constitute Air Force approval of the report's findings or conclusions. It is published only for the exchange and stimulation of ideas.

Michael Zambrana
SMC/AXE

REPORT DOCUMENTATION PAGE

Form Approved
OMB No. 0704-0188

1. REPORT DATE (*DD-MM-YYYY*)	2. REPORT TYPE	3. DATES COVERED *(From - To)*
15-04-2005		

4. TITLE AND SUBTITLE

Image Analysis Study of the Porosity Characteristics of Nickel Sinter

5a. CONTRACT NUMBER
FA8802-04-C-0001

5b. GRANT NUMBER

5c. PROGRAM ELEMENT NUMBER

6. AUTHOR(S)

A. H. Zimmerman and G. A. To

5d. PROJECT NUMBER

5e. TASK NUMBER

5f. WORK UNIT NUMBER

7. PERFORMING ORGANIZATION NAME(S) AND ADDRESS(ES)

The Aerospace Corporation
Laboratory Operations
El Segundo, CA 90245-4691

8. PERFORMING ORGANIZATION REPORT NUMBER

TR-2005(8555)-3

9. SPONSORING / MONITORING AGENCY NAME(S) AND ADDRESS(ES)

Space and Missile Systems Center
Air Force Space Command
2450 E. El Segundo Blvd.
Los Angeles Air Force Base, CA 90245

10. SPONSOR/MONITOR'S ACRONYM(S)
SMC

11. SPONSOR/MONITOR'S REPORT NUMBER(S)
SMC-TR-05-16

12. DISTRIBUTION/AVAILABILITY STATEMENT

Approved for public release; distribution unlimited.

13. SUPPLEMENTARY NOTES

14. ABSTRACT

A new image-analysis technique is described for measuring the distributions of irregularly shaped pores through the structure of porous electrodes. This technique has been used to measure the porosity characteristics of sintered nickel plaque made by a range of manufacturing processes for use in the nickel electrodes in nickel-hydrogen cells. These characteristics include variations in porosity and pore size through the thickness of the sinter, as well as the uniformity of the sinter. Sinter made using an aqueous slurry process is found to provide the uniformity typically found in dry-powder sinter processes, with the smaller pore sizes typically associated with the alcohol-based slurry sinter process.

15. SUBJECT TERMS

Sinter, Nickel electrodes, Nickel-hydrogen cells, Batteries, Porosity, Porosimetry

16. SECURITY CLASSIFICATION OF:			17. LIMITATION OF ABSTRACT	18. NUMBER OF PAGES	19a. NAME OF RESPONSIBLE PERSON
a. REPORT	b. ABSTRACT	c. THIS PAGE			Albert Zimmerman
UNCLASSIFIED	UNCLASSIFIED	UNCLASSIFIED		31	19b. TELEPHONE NUMBER *(include area code)* (310)336-7415

Contents

1. Introduction 1
2. Sinter Samples 3
3. Image Analysis Porosimetry Measurement Method 5
4. Unique Sinter Structures 11
   - 4.1 Unusual Sinter Voids 11
   - 4.2 Unusual Sinter Aggregates 14
5. Image Analysis Porosimetry Results 17
   - 5.1 Alcohol-Based Slurry Sintered Plaque 17
   - 5.2 Water-Based (Aqueous) Slurry Sintered Plaque 21
   - 5.3 Dry-Powder Sintered Plaque 23
6. Discussion of Results 29
7. Conclusions 31

References 33

Figures

1. Typical SEM image of a cross-sectioned plaque sample. 5
2. Distribution of the pixel luminosity over a typical 1280- by 960-μm SEM image of a cross-sectioned nickel plaque sample. 6
3. Illustration showing how ray length resolution is improved by adjusting the ray length to reflect the intensity gradient between adjacent pixels at the terminus of the ray 7
4. Colored-in pores located in a 1280 x 960 cross-section image of nickel plaque 8
5. Large void frequently seen in alcohol-based slurry sinter away from the center grid-containing region. 11

6. Large voids frequently seen in alcohol-based slurry plaque in proximity with the center grid wires. 12

7. Center void that has thinned down to appear more like a crack that is occasionally seen in slurry sinter. 12

8. Void commonly seen in dry powder nickel sinter where the powder has separated from the grid wires. 13

9. Horizontal crack or void occasionally seen on the side of dry powder sinter where there are no supporting grid wires. 14

10. High density aggregates of nickel powder frequently seen in alcohol-based slurry nickel sinter. 15

11. Surface aggregate or lump of high-density nickel powder seen infrequently (once) for water-based slurry nickel sinter 15

12. Nickel particles sintered into a closed-loop chain in a dry-powder sinter sample. 16

13. Needle-shaped nickel fragment seen in one sample of dry-powder nickel sinter. 16

14. Changes in the pore size distribution through the thickness of a typical sample of alcohol-based slurry plaque. These data are from sample 2D. 17

15. Variation in the average pore size through the thickness of alcohol-based slurry plaque samples from Group 1. 18

16. Variation in the average plaque porosity through the thickness of alcohol-based slurry plaque samples from Group 1. 18

17. Variation in the average pore size through the thickness of alcohol-based slurry plaque samples from Group 2. 19

18. Variation in the average plaque porosity through the thickness of alcohol-based slurry plaque samples from Group 2. 19

19. Variation in the average pore size through the thickness of alcohol-based slurry plaque samples from Group 3. 20

20. Variation in the average plaque porosity through the thickness of alcohol-based slurry plaque samples from Group 3. 20

21. Changes in the pore size distribution through the thickness of a typical sample of water-based (aqueous) slurry plaque 22

22. Variation in the average pore size through the thickness of water-based (aqueous) slurry plaque samples from Group 6. 22

23. Variation in the average plaque porosity through the thickness of water-based (aqueous) slurry plaque samples from Group 6. 23

24. Changes in the pore size distribution through the thickness of a typical sample of dry-powder plaque. These data are from sample 4A. 24

25. Variation in the average pore size through the thickness of dry-powder plaque samples from Group 4. 25

26. Variation in the average plaque porosity through the thickness of dry-powder plaque samples from Group 4 25

27. Variation in the average pore size through the thickness of dry-powder plaque samples from Group 5. 26

28. Variation in the average plaque porosity through the thickness of dry-powder plaque samples from Group 5 26

29. Variation of the average pore size (at 50% cumulative pore volume) for the different groups of plaque samples studied here. 29

30. Variability in pore size (as a percentage of overall average pore size) for each type of plaque. 30

31. Variability in plaque porosity (as a percentage of overall average sinter porosity) for each type of plaque. 30

Table

1. Sinter Samples Analyzed 3

1. Introduction

The nickel electrodes that are used in nickel-hydrogen cells require a well-made sintered nickel plaque as a substrate in their production. If the sintered nickel plaque contains large voids, surface protrusions, or other kinds of defects, it will not generally allow the production of high-performance nickel electrodes. A number of processes are presently used for producing the sintered nickel plaque used in nickel-hydrogen cells. The principal processes include:

Process 1: Alcohol-based slurry process

Process 2: Dry powder process

Process 3: Water-based, or aqueous slurry process

The slurry processes mix the nickel powder with pore-forming materials into either a water- or alcohol-based slurry that is coated with the desired thickness onto a nickel screen, dried, and sintered. The dry powder process covers the nickel screen with a prescribed thickness of dry nickel powder, which is directly sintered with no added pore forming components.

All three of these processes have been used to produce sinter that has been used in well-performing nickel electrodes. Each process has also been used to produce sinter having a range of thickness and overall porosity. The thickness range of sinter made by these processes is typically 0.030 to 0.036 in., and the range of porosities typically available is 76–84%.

Sinter made by any of these three processes is generally controlled to produce a sintered sheet having both the desired thickness and overall porosity, as well as an adequate bend strength. Any internal variations in pore size or porosity are not tracked or controlled, but simply emerge as the consequences of that particular production process and its process controls. Here we develop a new image analysis method that is capable of more accurately measuring the distributions of pore sizes in porous electrodes, which have highly irregular pore shapes and multiple interconnections between the pores. This method does not suffer from the systematic under-counting of small pores that occurs in line-scan methods that have been previously used,[1] and thus provides a better indication of the actual volume-based distribution of pore sizes in porous electrodes.

This new image analysis method has been used to measure variations in the internal pore characteristics of sinter made by all three of the processes described above. The objective of this study is to accurately measure systematic differences in the internal pore structure existing for nickel sinter made by each process.

2. Sinter Samples

A range of samples of various types of sintered nickel plaque was obtained for this study. The samples are listed and described in Table 1. For each sinter sample obtained for analysis, two pieces were cut from different parts of the sample and analyzed separately. The A and B pieces are from one sinter sample, while the C and D pieces (or E and F pieces) are from additional sinter samples. Each piece of sinter used for the analysis was approximately 1 in. by 0.5 in. in size. Table 1 reports the measured thickness and porosity for each analysis piece. The nominal thicknesses are 30 mils for all the slurry samples (except 36 mils for 6A and 6B, and 33 mils for 6C and 6D), and 35 mils for all the dry powder samples. The reported thickness measurements are the average of four measurements at different locations on each piece of sintered plaque. The nominal porosity is 76% for all slurry samples (except 78% for 6C and 6D) and 80% for all dry powder samples. The reported porosity of each piece was determined from its volume (based on the measured thickness, length, and width of each piece) and weight, and assuming that it was composed of pure nickel metal.

Table 1. Sinter Samples Analyzed

ID	Sample ID	Process	Thickness (mils)	Porosity (%)	Treatment
1A	4.5-in. coined sheet	Alcohol slurry	30.28	76.18 %	Oxidized
1B	4.5-in. coined sheet	Alcohol slurry	30.75	76.07	Oxidized
1C	3.5-in. coined sheet	Alcohol slurry	29.45	75.50	Oxidized
1D	3.5-in. coined sheet	Alcohol slurry	29.45	75.84	Oxidized
2A	L-439 C4	Alcohol slurry	31.50	76.02	Unoxidized
2B	L-439 C4	Alcohol slurry	30.51	75.53	Unoxidized
2C	L-439 C4	Alcohol slurry	31.69	76.27	Unoxidized
2D	L-439 C4	Alcohol slurry	30.67	75.66	Unoxidized
3A	L-438 C4	Alcohol slurry	29.65	76.09	Oxidized
3B	L-438 C4	Alcohol slurry	29.72	75.84	Oxidized
3C	L-438 C4	Alcohol slurry	29.41	76.02	Oxidized
3D	L-438 C4	Alcohol slurry	29.02	75.72	Oxidized
4A	L-0995	Dry powder	34.69	80.99	Unoxidized
4B	L-0995	Dry powder	34.72	81.16	Unoxidized
4C	L-0995	Dry powder	34.45	80.72	Unoxidized
4D	L-0995	Dry powder	34.21	80.15	Unoxidized
5A	L-0992	Dry powder	36.10	81.95	Oxidized
5B	L-0992	Dry powder	35.63	81.52	Oxidized
5C	L-0992	Dry powder	34.96	80.79	Oxidized
5D	L-0992	Dry powder	34.92	80.99	Oxidized
6A	60-05-135-0	Aqueous slurry	37.95	77.99	---
6B	60-05-135-0	Aqueous slurry	35.78	76.59	---
6C	60-05-125-0	Aqueous slurry	34.45	78.90	---
6D	60-05-125-0	Aqueous slurry	32.83	78.59	---
6E	60-05-113-0	Aqueous slurry	31.10	76.63	---
6F	60-05-113-0	Aqueous slurry	31.18	76.76	---

The porosities reported in Table 1 include the nickel screen that is imbedded within the sinter as an electrically conductive supporting structure. If this supporting screen is not considered in determining the sinter porosity, the porosity for the sinter alone is about 4% greater than that reported in Table 1. The lower porosity that includes the screen is referred to as the plaque porosity, while sinter porosity refers to the sinter without the imbedded screen. All porosimetry measurements reported in the following sections refer to the measured plaque porosity reported in Table 1.

3. Image Analysis Porosimetry Measurement Method

The pores within each sample of sintered nickel plaque were measured and analyzed using a method that actually measured the volume within each pore, based on analysis of images from the cross-sectioned pores. This method differs from line-scan techniques reported in References 1 and 2 in that this method measures and counts each pore detected in the cross sections rather than only those encountered during periodic line-scans across the cross-section.

Each sample was potted, cross-sectioned, and polished to enable high-quality images of the internal sinter to be obtained. However, rather than using piezoelectric positioners to automatically scan across the conductive features of the sinter as was done in Reference 2, Scanning Electron Microscopy (SEM) images of the plaque were obtained that provided good contrast between the nickel sinter particles and the pores between the sinter particles. These SEM images were obtained with a resolution of 1 μm, with each image showing a 1280-μm length of the plaque sample. A typical SEM image is indicated in Figure 1. Approximately 20 non-overlapping images such as that indicated in Figure 1 were required to completely image all pores across the 1-in. length of each cross-sectioned plaque sample. In these SEM images, the nickel screen wires show up as large white circles or ellipses, the nickel sinter particles as small white regions, and the pores as dark regions that are surrounded by the sinter particles.

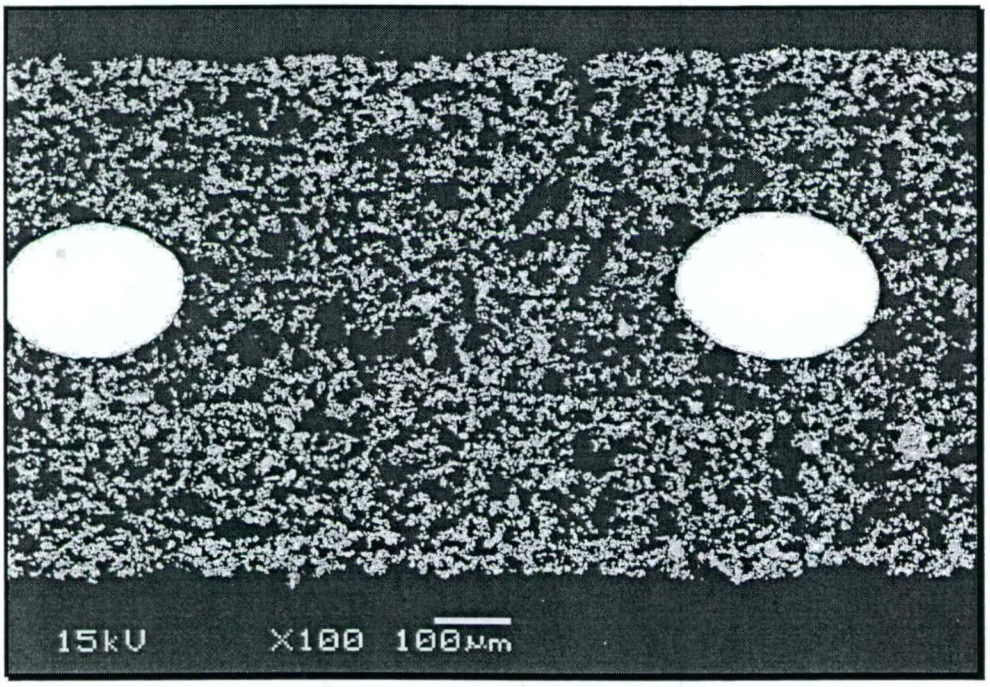

Figure 1. Typical SEM image of a cross-sectioned plaque sample.

The method used to detect and measure the pores in each plaque piece involved scanning the pixels over an imaged cross-section of the plaque, such as that in Figure 1 (without the labels at the bottom of the image). This image typically was 1280 pixels wide (x-direction) and 960 pixels in height (y-direction). The thickness of the image across the sample was determined at each x-location based on the maximum and minimum y-coordinates that were above an image-specific brightness threshold. These maximum and minimum levels were extended 25 μm to the left and right of the selected x-coordinate, thus allowing for surface roughness and surface pores up to 50 μm in diameter.

The brightness threshold was chosen for each image to discriminate between the nickel metal and the void regions. This threshold was chosen to correspond to the minimum in the distribution of pixel brightness that made up the plaque image, as indicated in Figure 2 for a typical sample. The average porosity throughout the entire sample was determined by the ratio of the pixels within the sectioned image that were below the brightness threshold to the total number of pixels between the maximum and minimum extremes of the image.

To locate a pore, the pixels in the sample image region were scanned until a pixel was located that had an intensity below the brightness threshold, thus indicating that this pixel location was within a pore. The first task is to determine the location of the center of the pore since the initial pixel found could be at any random location within the pore. The center of the pore was located by following 360 rays outward from the initially found pixel location, with each ray originating at the initially found pixel location. These rays spread in all directions, in 1° angular increments, for the purpose of probing the local structure around the initial pixel. Each ray is extended in length until it encounters a pixel that is above the brightness threshold, or it encounters the upper or lower surfaces of the sample.

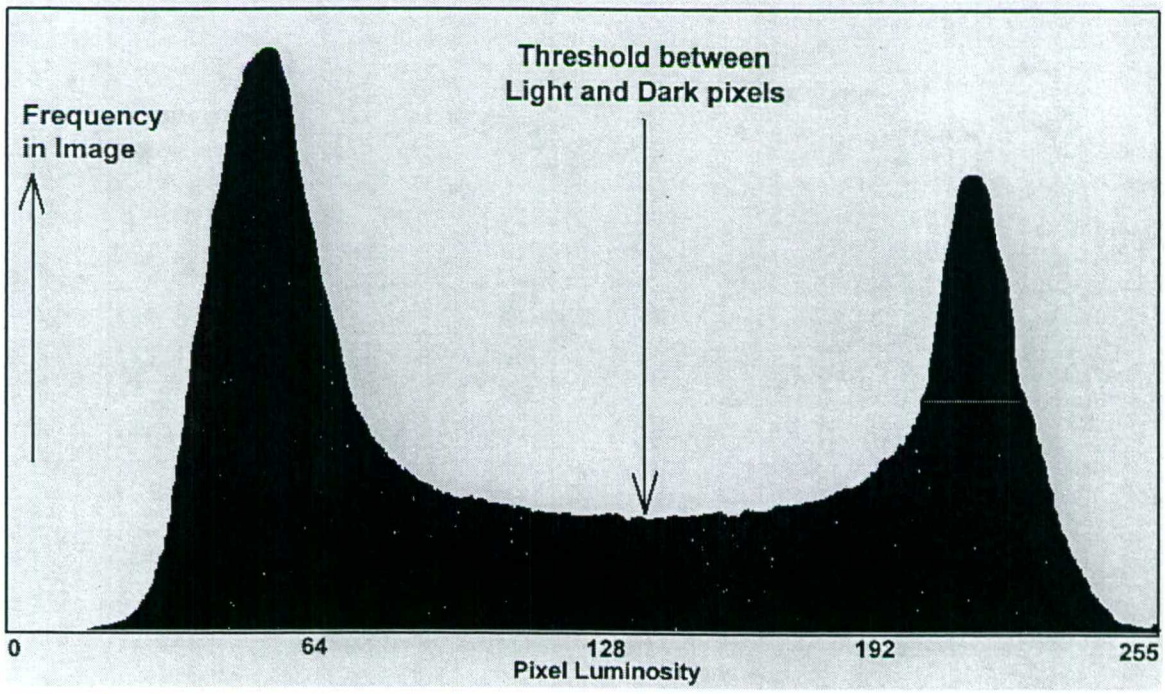

Figure 2. Distribution of the pixel luminosity over a typical 1280- by 960-μm SEM image of a cross-sectioned nickel plaque sample.

The average x and y components of all 360 rays provide a first-order location for the center of the pore. The ray-tracing procedure is repeated from the new center location, which provides an improved determination of the center location of the pore. Four complete ray-tracing iterations are performed to accurately find the center of the pore based on its local boundary structure. If any of the rays used to determine the pore location encounters the left or right boundaries of the cross-section, the pore is ignored because the image contains insufficient information to determine the pore location.

Once the center of a pore has been iteratively located, the size of the pore can be determined based on the local porous structure surrounding the pore. To determine the pore size, we again use the ray-tracing technique described above; however, the origin for the rays that probe the local porous structure is now the center of the pore. Again, if any ray encounters the upper or lower surfaces of the sample, it is truncated. In addition, if any ray encounters the left or right boundaries of the cross-section, the pore is ignored because the image contains insufficient information to correctly determine the pore size. The overall pore radius is taken to be the average of the lengths of the 360 rays emanating from the center of the pore to the nearest above-threshold pixel.

Because the pixels in each image typically have a 1-μm resolution, the maximum pore size resolution that can be obtained is seemingly the same as the image resolution (1 μm). However, the pixels in the image also contain intensity information that, if properly analyzed, can provide significantly improved resolution for the location of the threshold boundary between adjacent pixels. It is the location of this threshold boundary that determines the pore boundary, and thus the pore size. This boundary location was determined at the terminus of each ray by interpolation of intensity between a pixel that was below the threshold intensity and an adjacent pixel that was above the threshold intensity. Figure 3 graphically illustrates this interpolation procedure. If the intensity resolution of the pixels that comprise the image is 256 (i.e., a 256-color gray-scale image with 1-μm resolution per pixel), the interpolation procedure yields an actual size resolution of about 0.1 to 0.01 μm, depending

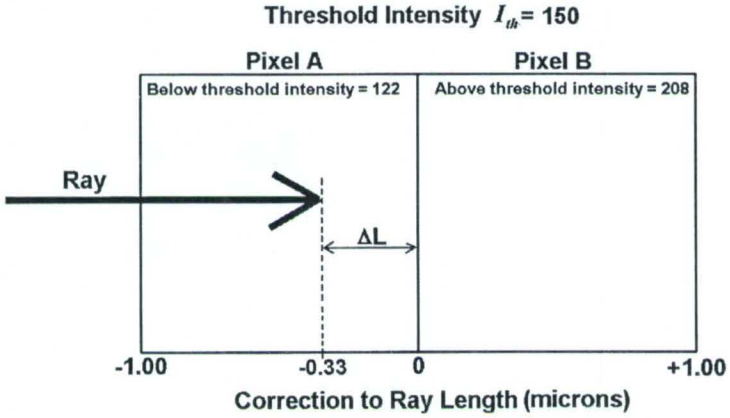

$$\Delta L = \frac{I_{th} - I_a}{I_b - I_a} = \frac{150 - 122}{208 - 122} = 0.33$$

Figure 3. Illustration showing how ray length resolution is improved by adjusting the ray length to reflect the intensity gradient between adjacent pixels at the terminus of the ray. In this example, the ray length is 0.33 μm less than if it were taken to be simply the boundary between the pixels.

on the intensity gradient between the adjacent pixels at the terminus of each ray. Of course, the actual resolution also depends on the sharpness and focus in the SEM images as well.

Once a pore has been found and its size determined, the pixels that comprise this pore must be marked so that they will not be included in locating or sizing adjacent pores. This is accomplished by coloring the pixel making up the pores with a new color specific to each pore that is located. The total number of pixels marked with this color is equal to the number expected for a pore with a circular cross-section having the average radius determined above (but not less that one pixel per pore). Since the pores generally have an irregular shape, the pixel-coloring process starts with the center pixel, and then proceeds in a circular pattern having an ever-increasing radius until the needed number of sub-threshold pixels are colored. The radius used in this pore-coloring operation is weighted by the square root of the ray radius within the angular region of each ray (as determined in the pore sizing operation). This allows the pore shape to diffuse irregularly into the porous structure according to the ditance to the nearest pore boundaries, and thus to conform to the complex shape of the porous substrate. Figure 4 shows the colored-in pores located for a typical image of a nickel plaque sample, both at 1280 x 960 μm resolution as well as a zoom-in of the pores in a much smaller region.

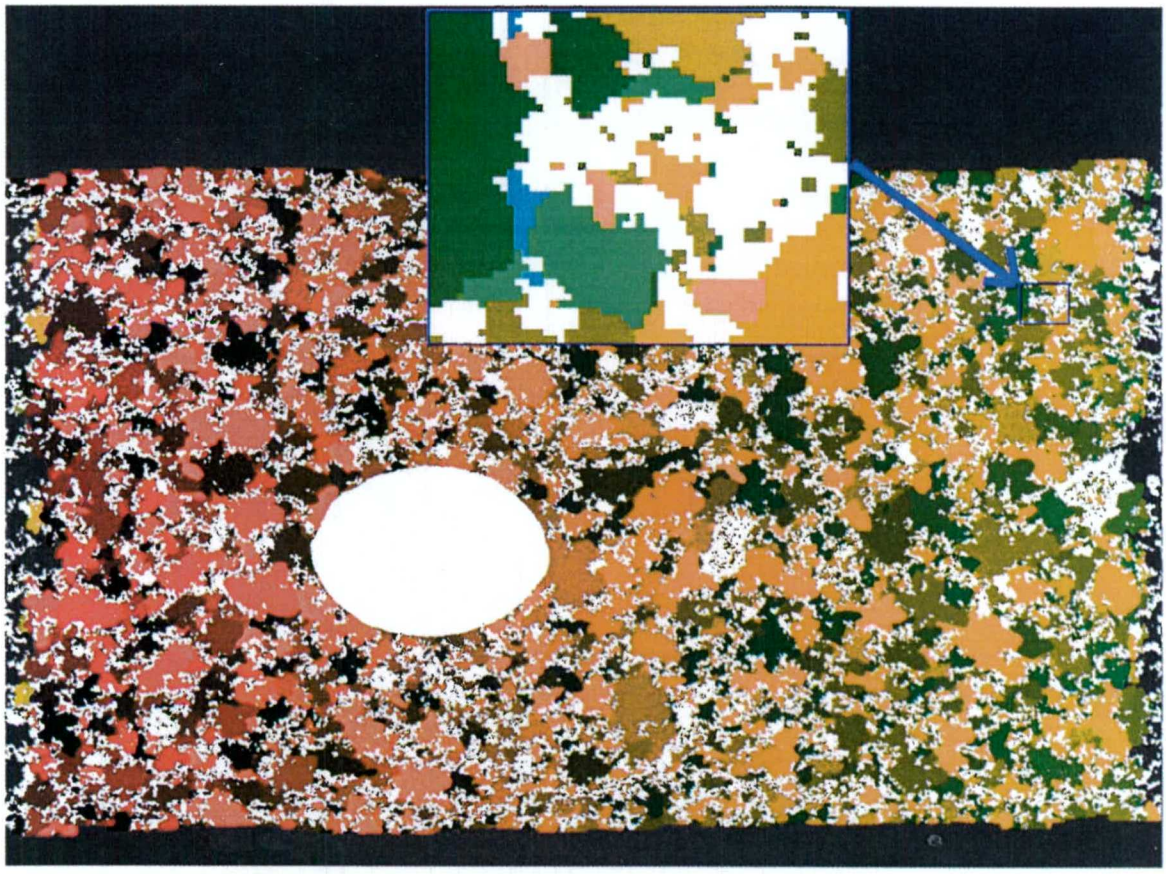

Figure 4. Colored-in pores located in a 1280 x 960 cross-section image of nickel plaque. White pixels are nickel metal. The magnified region shows individual pores highlighted with contrasting colors to allow them to be easily distinguished. Over 36,000 pores were located in this image.

The entire image analysis and pore location procedure described above was automatically performed on a series of 20–22 images that spanned each 1-in.-long cross-sectioned sample. The procedure typically detected 25,000 to 30,000 pores of various sizes ranging from 0.001 to over 100 μm in diameter. For each pore that was located, its radius, image name, center x and y coordinates, and pore number were all saved for follow-on analysis, if required. The pores were accumulated and sorted by size into 10 bins that corresponded to different locations through the thickness of the plaque. Bins 1 and 10 corresponded to the surface regions on each side of the plaque, while bin 5 corresponded to the center of the plaque. The location of the center of each pore dictated the bin into which it was placed. These ten bins thus provide an indication of how uniform the pore characteristics are through the thickness of the plaque.

The average porosity in each bin or in the overall sample was determined by the relative number of pixels below the brightness threshold. The average pore size was taken to the pore diameter at which 50% of the overall pore volume in a particular bin or the overall sample was in pores having a smaller diameter than the average, while the other 50% of the overall pore volume was in larger pores. The pore non-uniformity was taken to correspond to the percent variation of the pore size through thickness of a sample from the sample average pore size. The distributions of average pore size, average porosity, or pore uniformity through the plaque thickness are evaluated and examined here, along with the changes in the pore size distribution through the plaque.

4. Unique Sinter Structures

A number of unusual or unique structural features were seen when analyzing the SEM images during this study. The sinter shown in Figure 1 is typical of a relatively uniform and desirable structure. The types of departure from this relatively uniform structure, which are in some cases key factors in dictating the porosity characteristics, can be classified into either abnormal voids or abnormal nickel aggregates. Each of these types of features will be shown and discussed here, along with an indication of what types of plaque showed each condition and how frequently it was seen.

4.1 Unusual Sinter Voids

The type of void that was most often found to influence the pore size distribution was the large internal void. Thise type of void was seen exclusively in slurry plaque, and seen with much greater frequency in the alcohol-based slurry plaque. These voids may be classified as voids associated with central grid wires in the plaque, or large voids away from the center of the plaque and its supporting grid structure. The former type of void is shown in Figure 5, while the latter type is shown in Figure 6.

The large voids shown in Figures 5 and 6 are particularly undesirable because if they are loaded with nickel electrode active material, the active material is not very well utilized for storing energy because of the large distance through the active material to the nearest conductive metal surfaces. If the voids are not loaded with active material, the pores must be over-loaded elsewhere to provide the

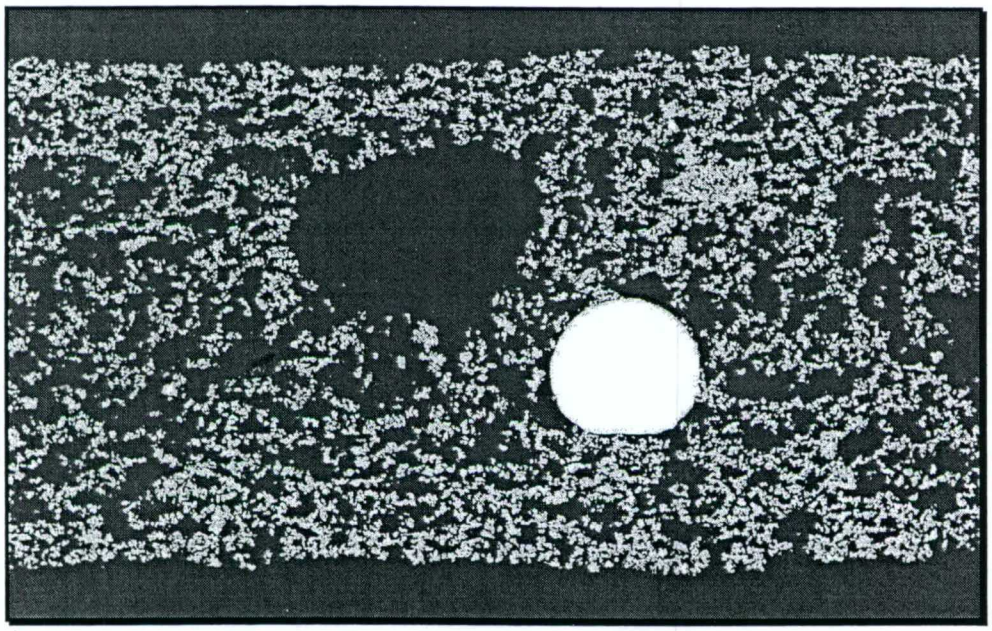

Figure 5. Large void frequently seen in alcohol-based slurry sinter away from the center grid-containing region.

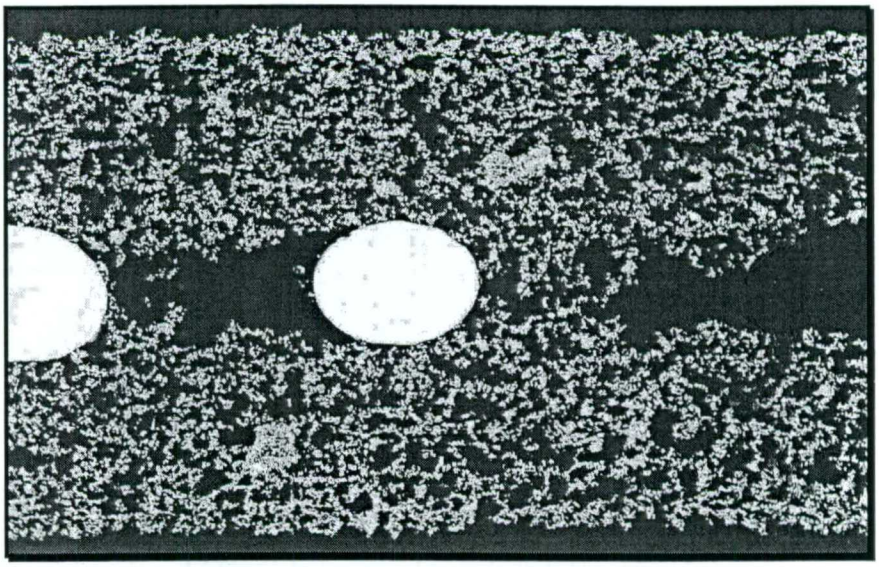

Figure 6. Large voids frequently seen in alcohol-based slurry plaque in proximity with the center grid wires.

correct average amount of active material. Typically, nickel electrodes made from plaque having large internal voids exhibit a significantly lower utilization than can be obtained with a uniform plaque. The large voids can also act as stress points within the finished nickel electrode where blisters can form, or the sinter can delaminate from the grid after long-term electrode operation. In several instances, the large voids seen in Figure 6 appeared to be reduced in thickness to where the void appeared more as a crack along the center line where the grid wires were situated in the plaque, as shown in Figure 7

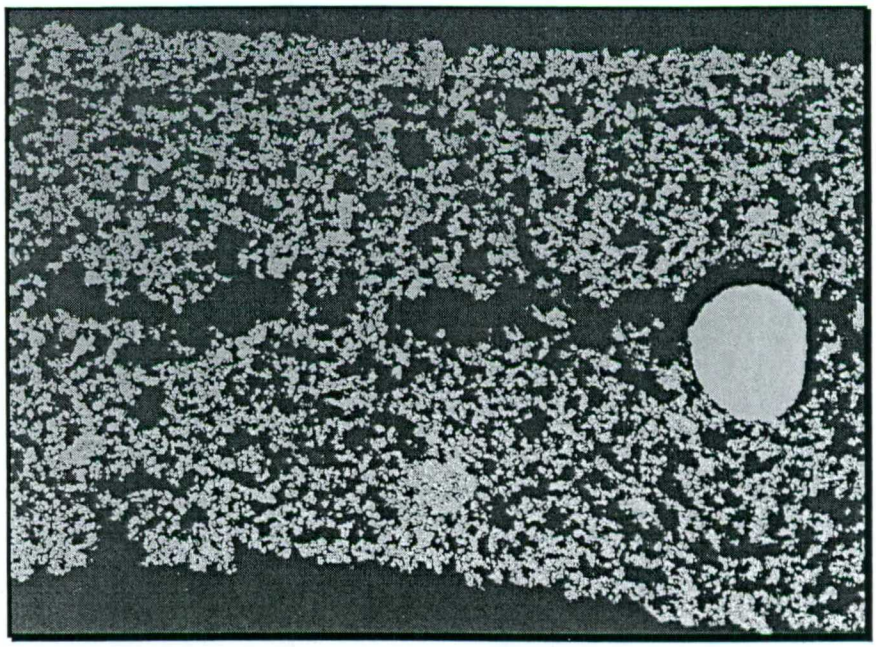

Figure 7. Center void that has thinned down to appear more like a crack that is occasionally seen in slurry sinter.

Voids within the sinter were also seen in dry powder plaque, although these voids typically had an appearance different from those in slurry plaque (Figures 5 through 7). In dry powder plaque, the most common type of void is seen immediately around a portion of the grid wires, where it appears that the nickel powder separated from the grid wire prior to or during the sintering operation. This type of void is shown in Figure 8. While this kind of void tends to cause the same type of reduced nickel electrode utilization that large voids cause in slurry plaque, it can provide an oxygen flow path from the interior of the nickel electrode to the outer surface. In dry powder plaque, the grid wire structure is generally situated at one edge of the plaque, thus any significant voids around these grid wires are often open to the electrode surface, as is the case in Figure 8. One can often visually see the exposed grid wires through such voids on the surface of the plaque. This type of surface void is why the screen side of dry powder plaque is positioned so that it does not face the separator in nickel-hydrogen cells.

The second type of void that is occasionally seen in dry powder plaque is a crack in the sinter, an example of which is shown in Figure 9. These cracks appear in most instances to have formed before the powder was sintered since there is no evidence of actual breaking of the necks between the nickel particles, and is probably caused by movement of the powder layers prior to sintering. These cracks can act as stress points where blisters form in finished nickel electrodes

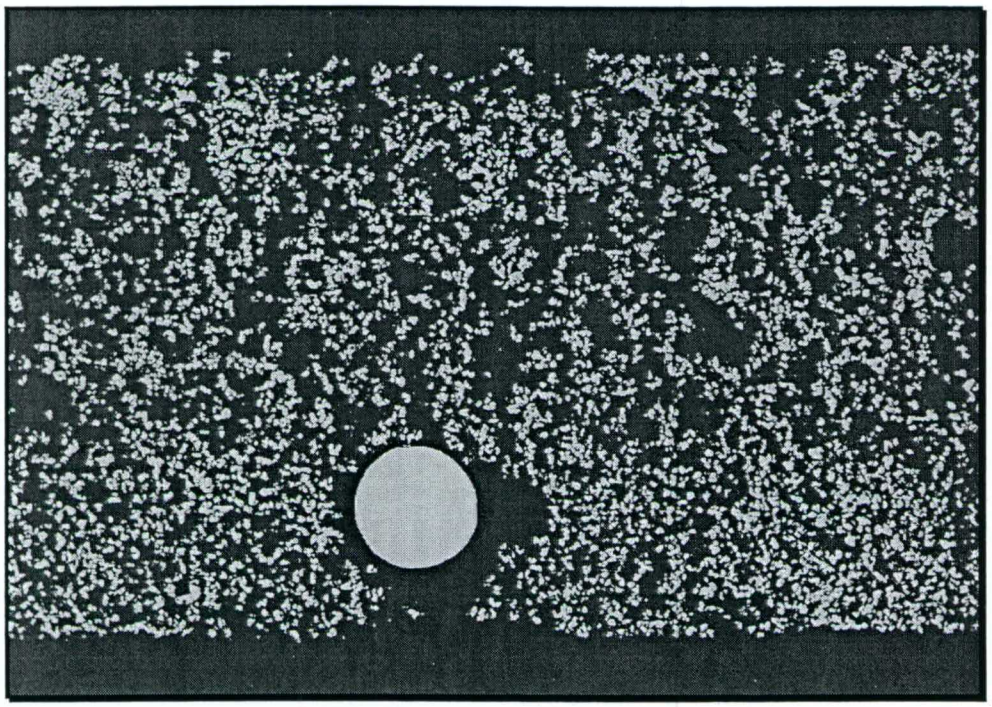

Figure 8. Void commonly seen in dry powder nickel sinter where the powder has separated from the grid wires.

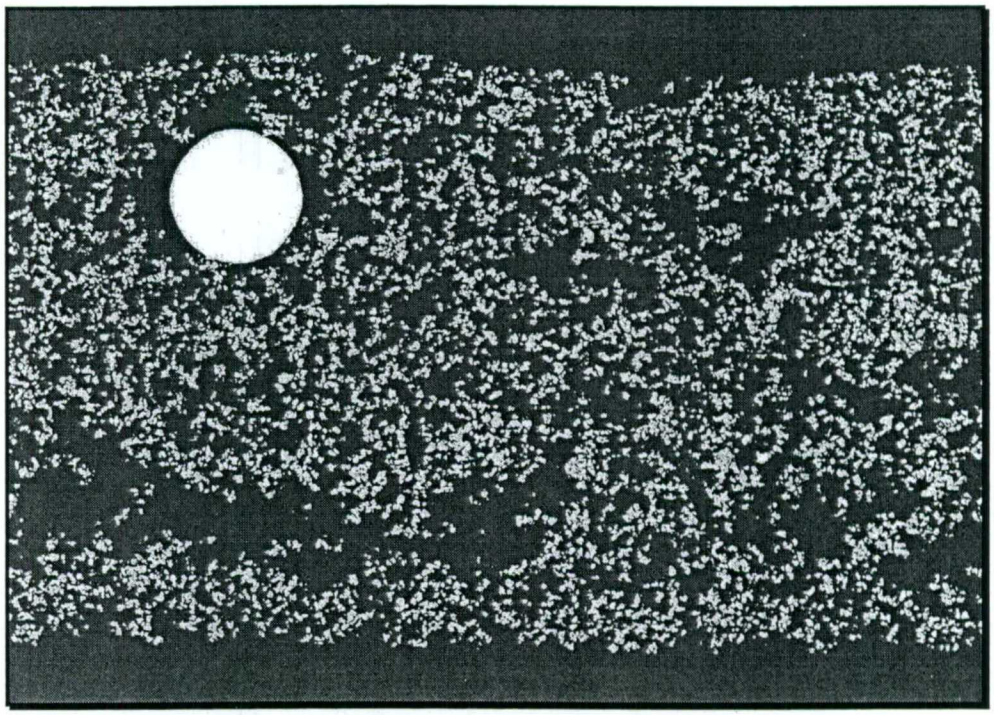

Figure 9. Horizontal crack or void occasionally seen on the side of dry powder sinter where there are no supporting grid wires.

4.2 Unusual Sinter Aggregates

In addition to voids in nickel plaque, undesirable aggregates of nickel powder are also sometimes seen. The most common type of aggregate is a region of high-density nickel powder that is imbedded within the plaque. An example is shown in Figure 10 for an alcohol-based slurry plaque sample, which is the type of plaque that most commonly displays this type of aggregate. Aggregates of this type were much less common in the waster-based slurry plaque samples, and when seen, tended to be significantly smaller than those shown in Figure 10. Aggregates of the type shown in Figure 10 mean that there are lower density regions elsewhere in the plaque if it is manufactured to the required overall porosity. The lower density regions (which often include larger voids) will tend to be loaded with more active material than the high-density regions shown in Figure 10, but will have lower utilization and thus reduce the overall utilization of the nickel electrode. One unusual aggregate was seen protruding from the surface of a water-based slurry plaque sample, as shown in Figure 11. A protruding aggregate of this type is a concern because it can cause a stress point on the separator in a cell stack, potentially increasing the probability of separator damage and the formation of a short circuit.

Aggregates of nickel in dry powder plaque have a quite different appearance that those illustrated in . The most common type of aggregate in dry-powder plaque is an extended chain of nickel particles that have been sintered into loops having either open (most common) or closed geometry. An example of a closed-loop aggregate is shown in the bottom-center region of Figure 12. While these chains and looped chains of nickel can be as large as 50 μm, they are not expected to have a significant effect on the performance of the dry-powder plaque because they do not appear to significantly alter the sizes or distributions of pores within the plaque.

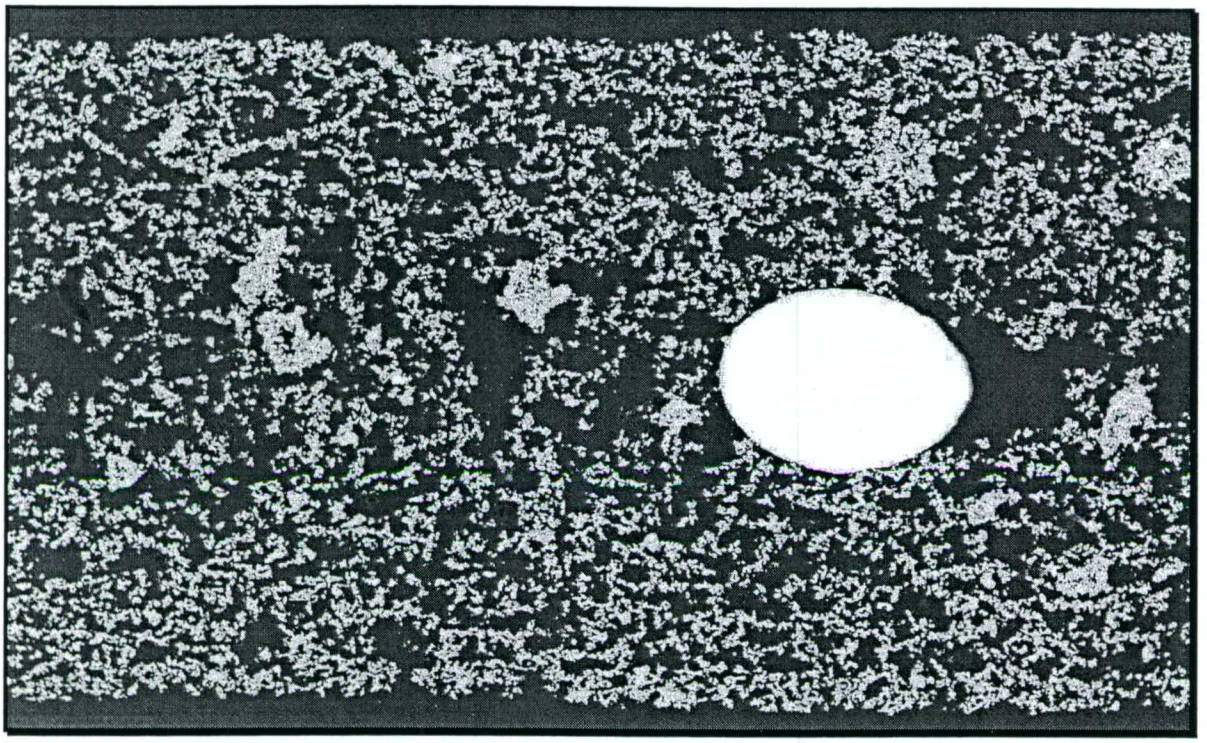

Figure 10. High density aggregates of nickel powder frequently seen in alcohol-based slurry nickel sinter.

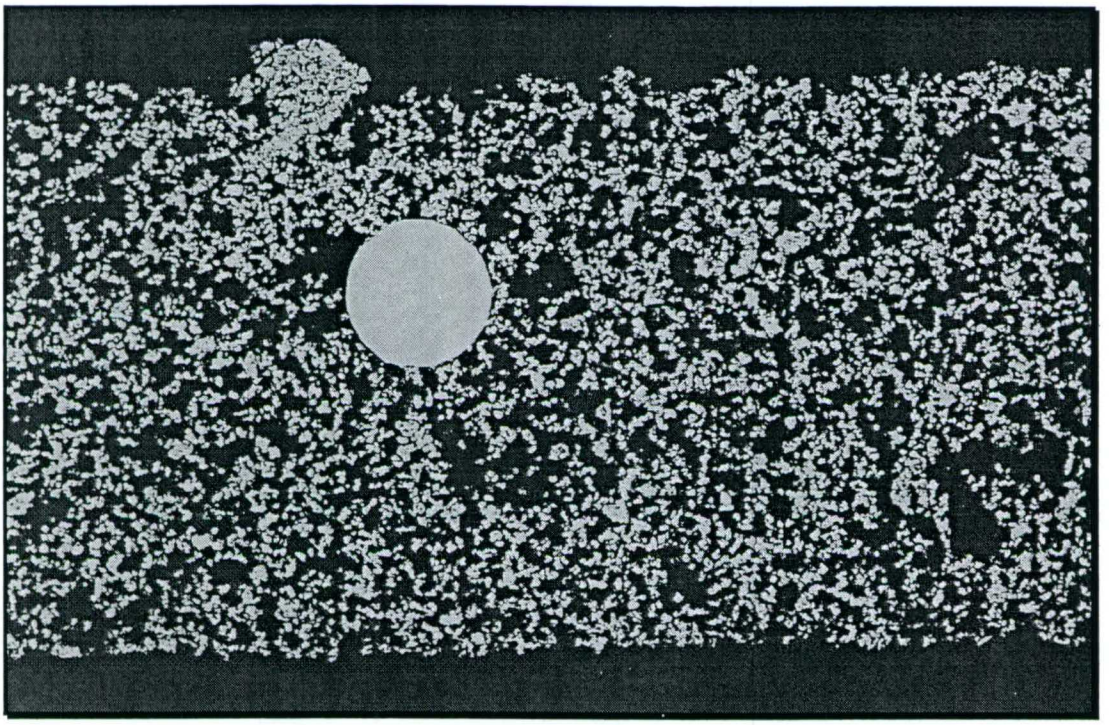

Figure 11. Surface aggregate or lump of high-density nickel powder seen infrequently (once) for water-based slurry nickel sinter.

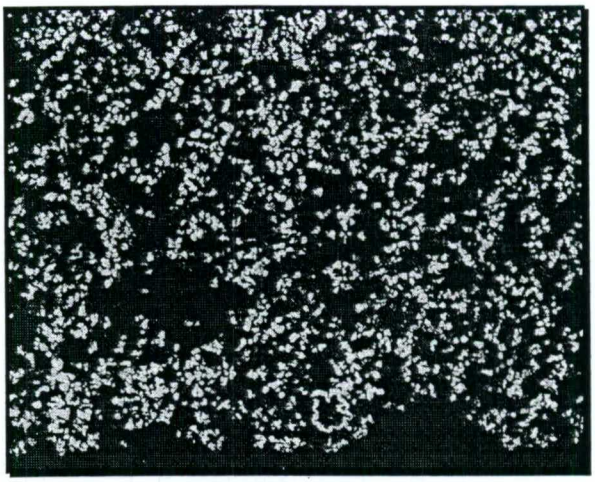

Figure 12. Nickel particles sintered into a closed-loop chain in a dry-powder sinter sample.

An example of an unusual aggregate was observed in a sample of dry-powder plaque. This aggregate appeared as a needle-like particle of solid nickel metal, and is shown in the bottom-center region of Figure 13. It is not clear whether this was a large pre-sintering fragment of metal, or whether it is simply a mass of smaller particles that were melted into a larger particle having a quite unusual and regular shape.

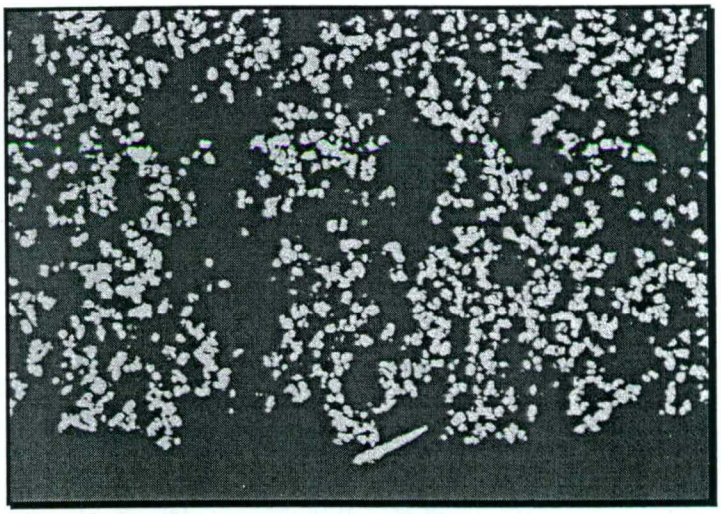

Figure13 . Needle-shaped nickel fragment seen in one sample of dry-powder nickel sinter.

5. Image Analysis Porosimetry Results

The image analysis porosimetry methodology described in Section 3 was performed for all the plaque samples summarized in Table 1, providing the distribution of pore volume as a function of pore size within each of ten regions through the thickness of each plaque sample. These pore size distributions reveal how the internal pore volume is distributed between differing types of pores in the samples. It is possible that some regions can exhibit bi-modal size distributions, while others can exhibit distributions where the pore volume is mostly in a few large voids, while other samples may exhibit quite uniform distributions throughout their thickness. In general, it is desirable to have relatively uniform distributions of pore volume. In addition, the average pore size and the average plaque porosity may be determined from the pore size distributions through the thickness of each plaque sample. In this section, the detailed results of the porosimetry analyses obtained from the complete analysis of all cross-sectioned pores are described for each sample from the alcohol-based slurry plaque, the water-based slurry plaque, and the dry powder plaque.

5.1 Alcohol-Based Slurry Sintered Plaque

As indicated in Table 1, twelve samples of alcohol-based slurry plaque were analyzed. The typical variation in pore size distribution through the thickness of these samples is shown in Figure 14. The most noteworthy characteristic of these distributions is the large increase in the pore sizes toward the

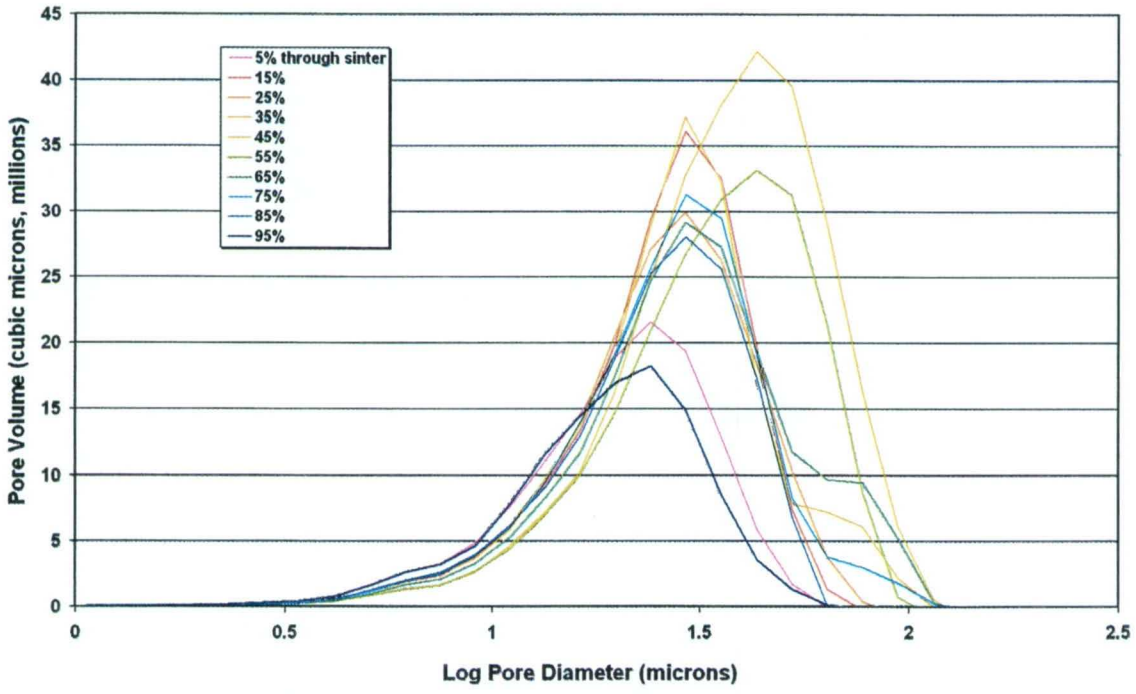

Figure 14. Changes in the pore size distribution through the thickness of a typical sample of alcohol-based slurry plaque. These data are from sample 2D.

center of the sample. This change is entirely due to the large voids seen in this type of slurry, and which are illustrated in Figures 5 and 6.

The changes in the pore size distributions are more easily compared for the different plaque samples by plotting the average pore size and the average porosity as a function of the plaque thickness. These plots are shown in Figures 15 through 20 for the alcohol-based slurry plaque samples in Groups 1 through 3.

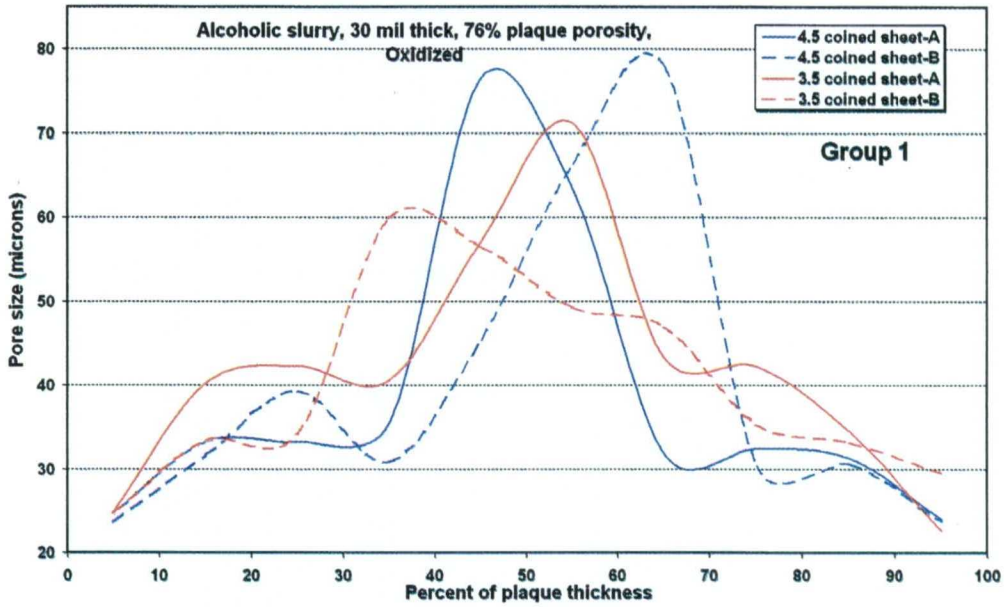

Figure 15. Variation in the average pore size through the thickness of alcohol-based slurry plaque samples from Group 1.

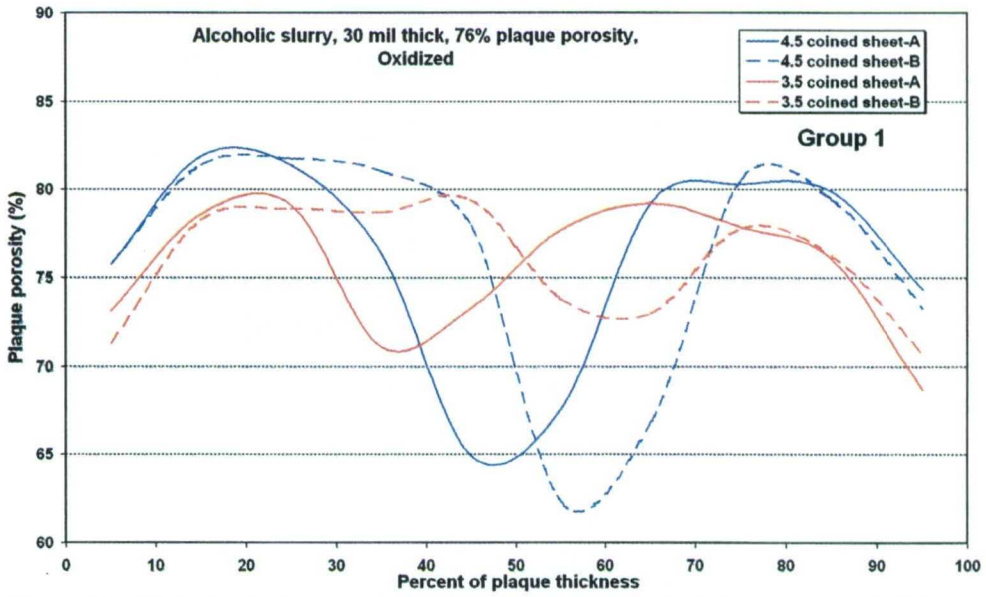

Figure 16. Variation in the average plaque porosity through the thickness of alcohol-based slurry plaque samples from Group 1.

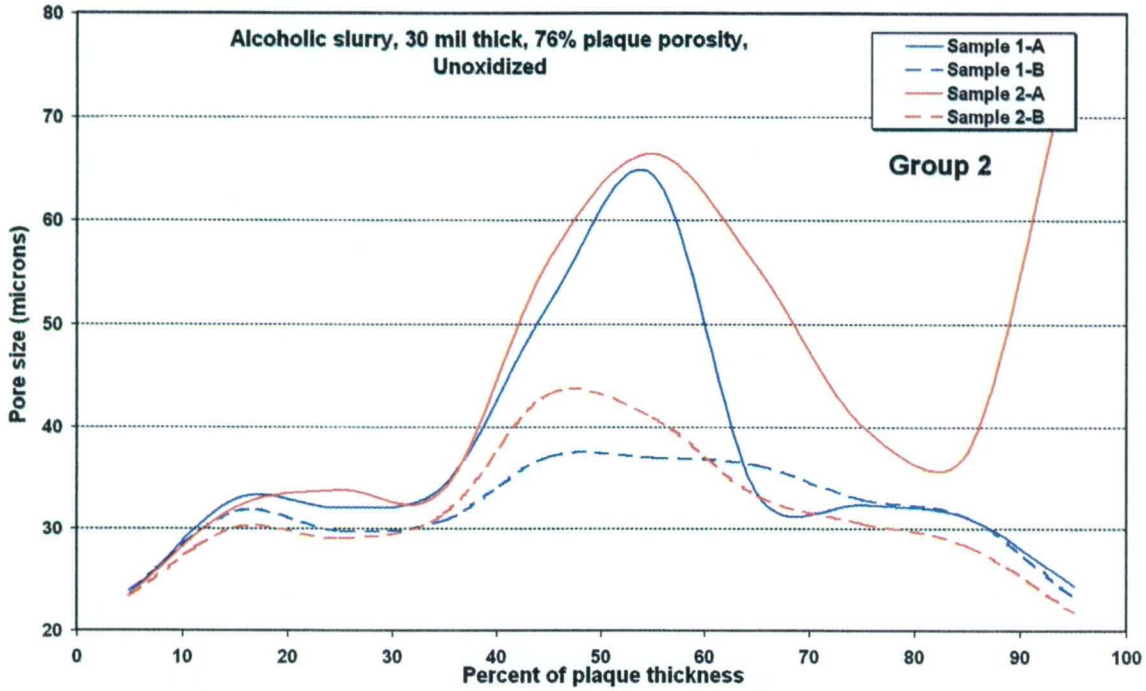

Figure 17. Variation in the average pore size through the thickness of alcohol-based slurry plaque samples from Group 2.

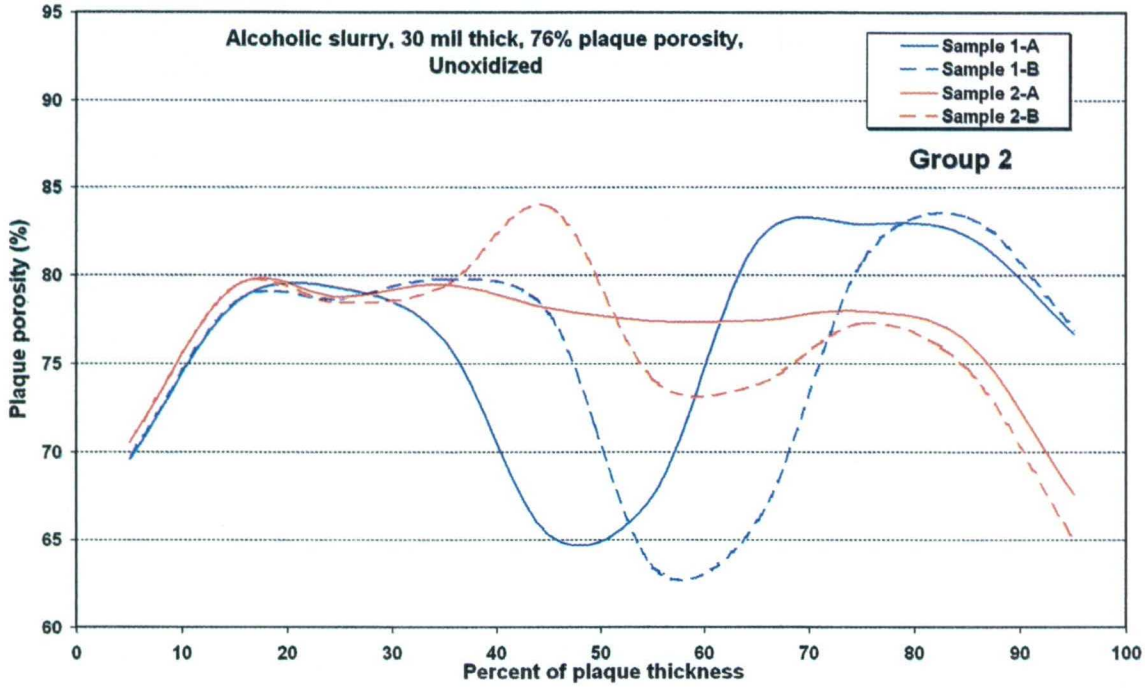

Figure 18. Variation in the average plaque porosity through the thickness of alcohol-based slurry plaque samples from Group 2.

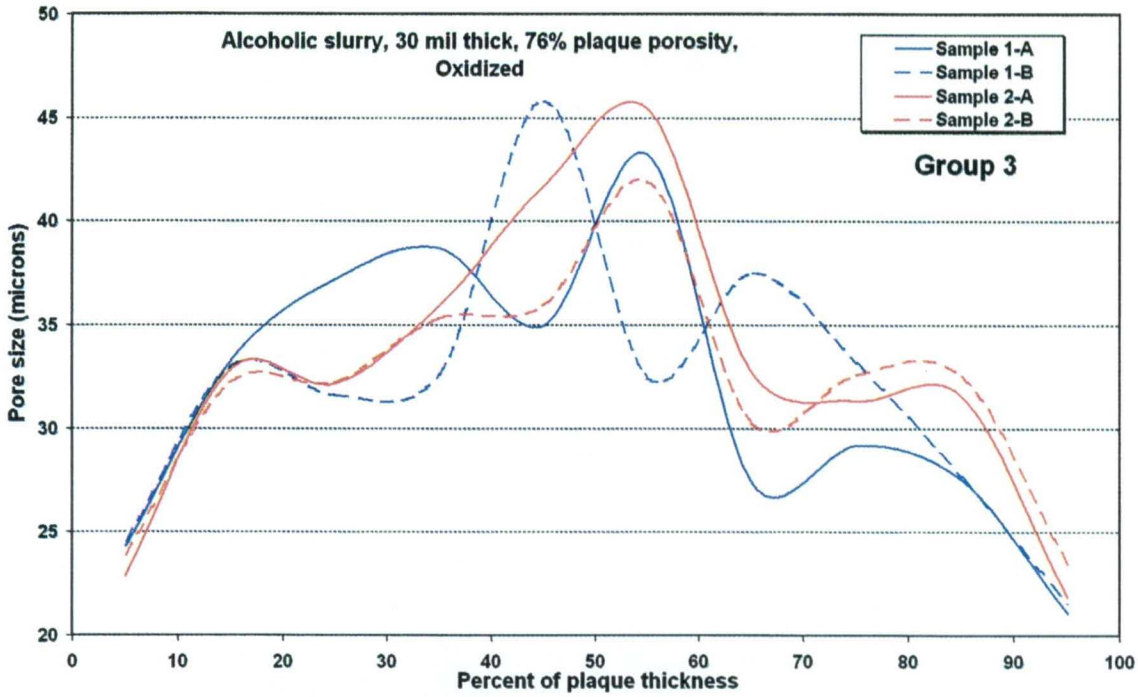

Figure 19. Variation in the average pore size through the thickness of alcohol-based slurry plaque samples from Group 3.

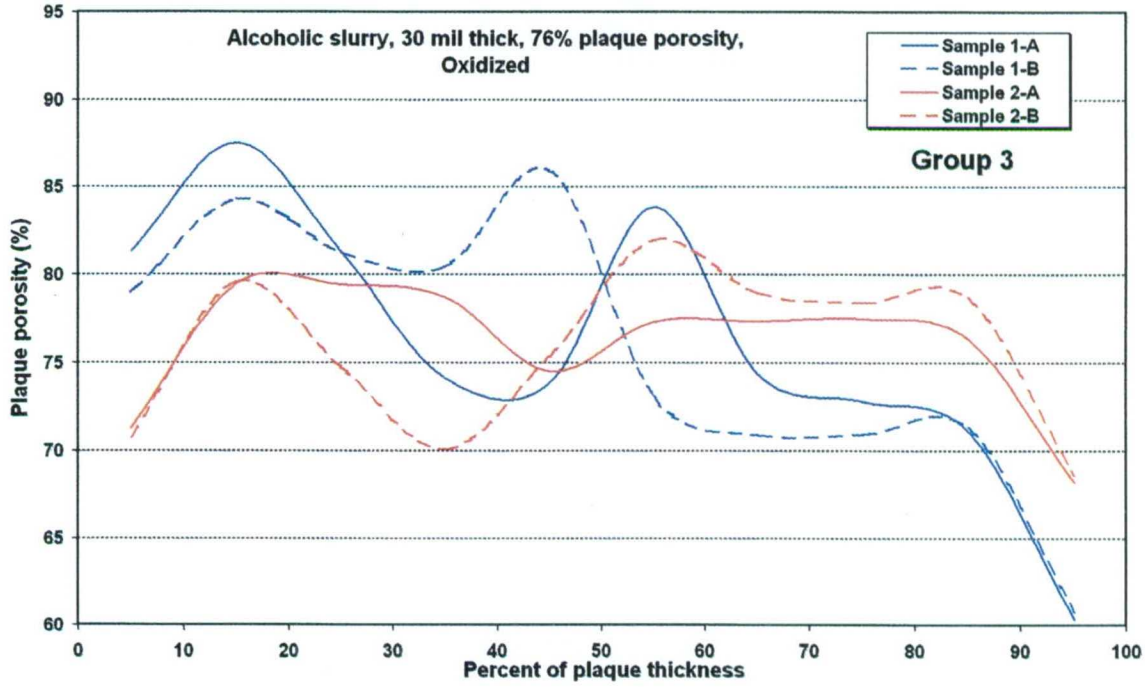

Figure 20. Variation in the average plaque porosity through the thickness of alcohol-based slurry plaque samples from Group 3.

The most significant variation in pore characteristics in these alcohol-based slurry samples is the large increase in average pore size at the center of the plaque in many (but not all) of the samples analyzed. This peak arises from the large voids that frequently are seen at the center of the sintered plaque, often in association with the location of the nickel screen wires. These voids are, however, not always present, as can be seen in Figure 17 where only one of the pieces cut from each sinter sample had the large internal voids. In the areas where the large internal voids were detected, the average pore size near the center of the sinter exceeded 70 μm, while in the areas that did not display the large internal voids, the average pore size near the center of the sinter was about 40 μm. While these variations in internal pore size are likely to cause a noticeable decrease in the utilization of nickel electrodes made from this plaque, historically slurry sinter plaque that contains large internal voids has been used to produce acceptably performing nickel electrodes.

The average porosity of the plaque samples in these three groups shows several features of interest. First, while the samples having large internal voids also have higher sinter porosity in the regions where the large voids occur, the presence of the dense grid wires often makes the overall plaque porosity lower in these regions. The second signature, which is characteristic of slurry sinter in general, is the decrease in average porosity at the surfaces of the sinter. Slurry sinter always seems to have a "skin" of higher density sinter at its surfaces. This characteristic lends it some added strength and can also act to prevent active material from being easily extruded from the pores at the "skin" of the sinter.

These results suggest that alcohol-based slurry sinter plaques of the types analyzed here consist of a composite of many regions containing large internal voids and some other regions containing a relatively uniform pore distribution through the plaque thickness. In the regions with large voids, the average pore size can exceed 70 μm at the center of the plaque. In the regions with uniform pore size distributions, the pore sizes typically range from 30 to 40 μm through the thickness of the plaque. The slurry sinter plaque also typically exhibits a skin having pore sizes of about 20 μm.

Comparison of the oxidized to the un-oxidized plaque samples indicated that the oxidation process did not significantly affect the porosity or pore size characteristics.

5.2 Water-Based (Aqueous) Slurry Sintered Plaque

As indicated in Table 1, six samples of water-based slurry plaque were analyzed. The typical variation in pore size distribution through the thickness of these samples is shown in Figure 21. In this figure, the plaque appears to have a relatively uniform distribution of pore sizes throughout its thickness. The width of this distribution is essentially independent of the location through the plaque thickness. However, the distribution moves up to slightly larger average pore sizes toward the center of the plaque, and is shifted downward to slightly smaller average pore sizes in the "skin" at the surface of the plaque. The total variation in pore size at the peak of the distributions in is from about 28 μm at the surface to about 33 μm in the center.

The changes in the pore size distributions are more easily compared for the different plaque samples by plotting the average pore size and the average plaque porosity as a function of the plaque thickness. These plots are shown in Figures 22 and 23 for the water-based slurry sinter plaque samples of group 6.

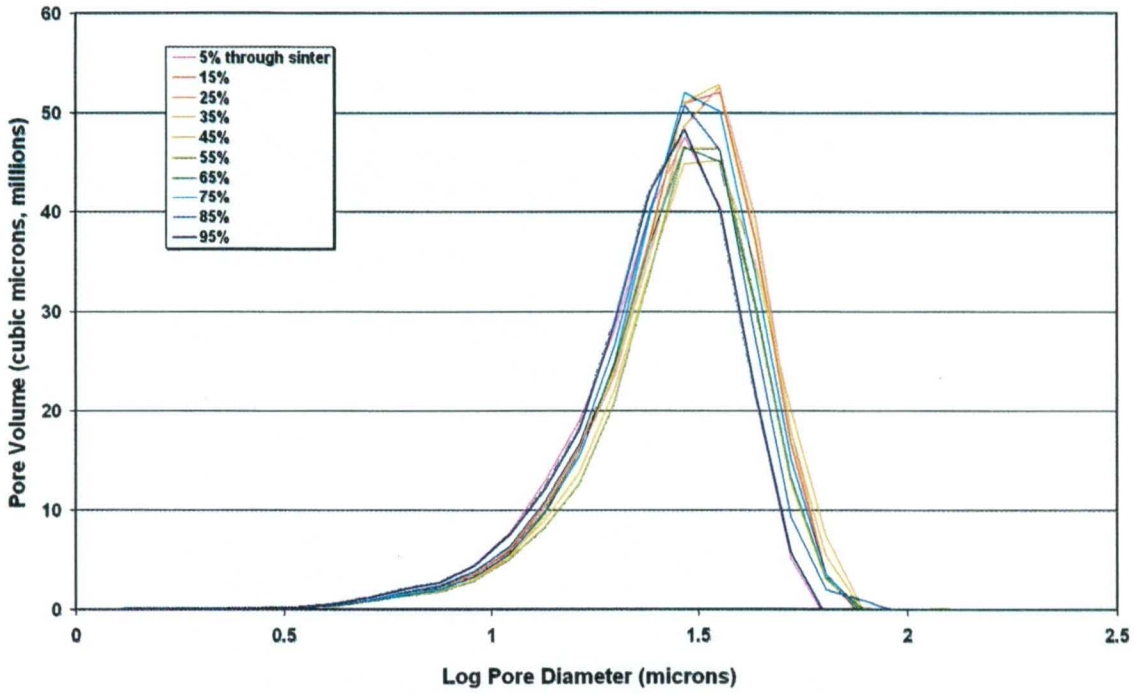

Figure 21. Changes in the pore size distribution through the thickness of a typical sample of water-based (aqueous) slurry plaque. These data are from sample 6D.

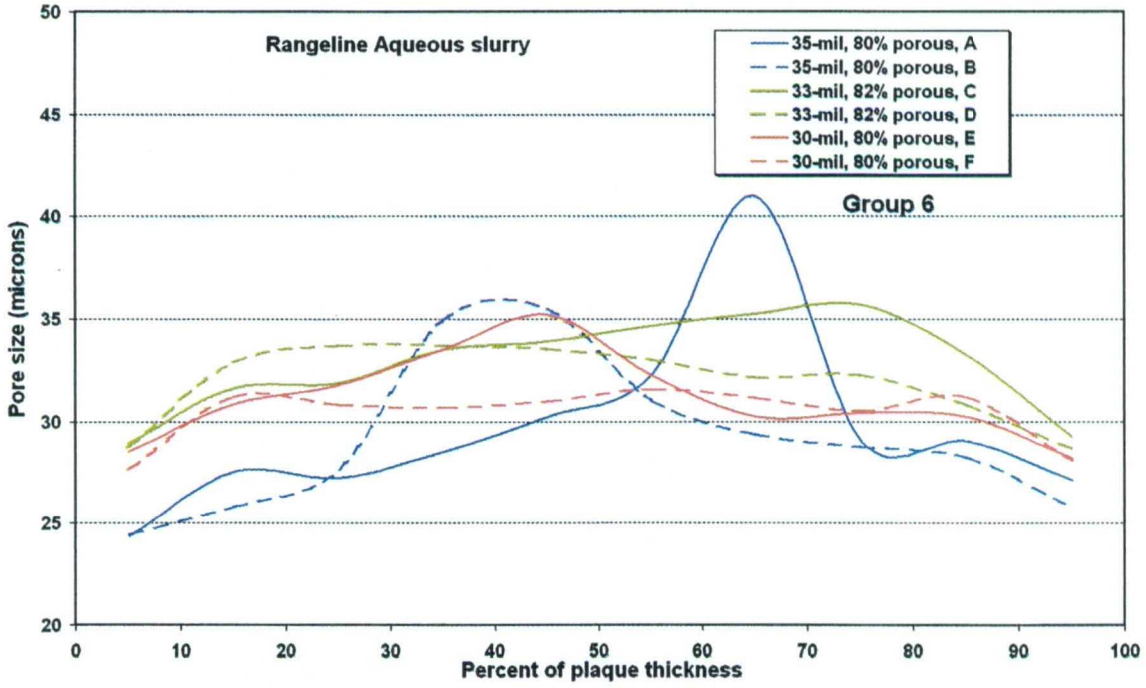

Figure 22. Variation in the average pore size through the thickness of water-based (aqueous) slurry plaque samples from Group 6.

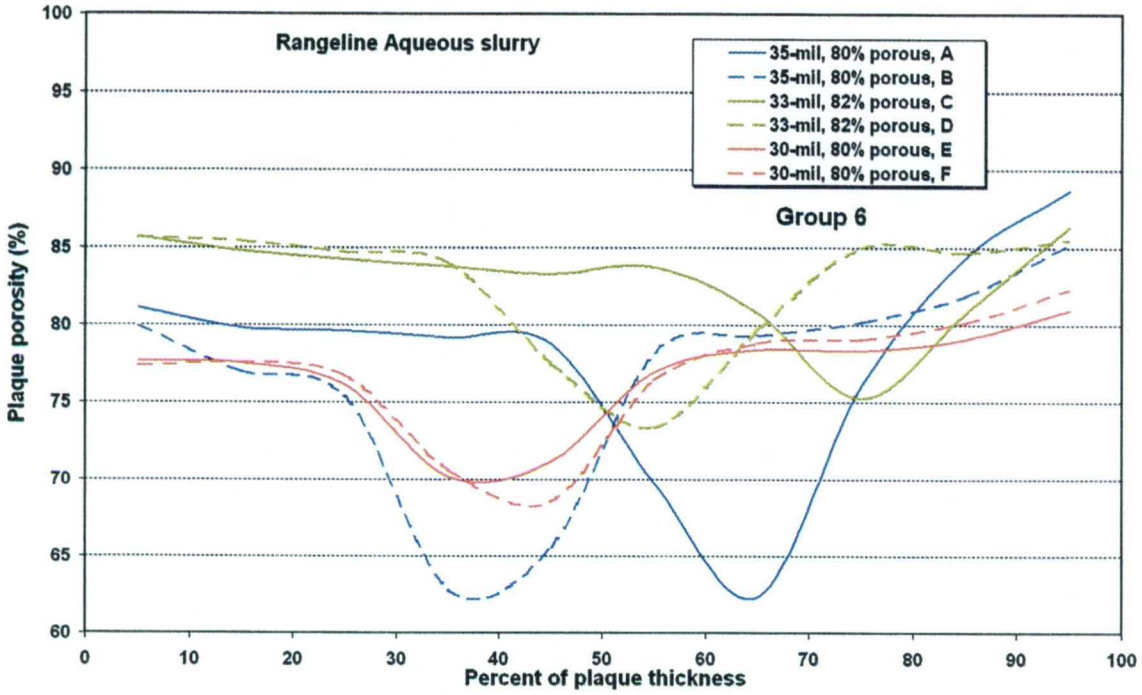

Figure 23. Variation in the average plaque porosity through the thickness of water-based (aqueous) slurry plaque samples from Group 6.

In comparison with the alcohol-based slurry samples, the water-based slurry appears to be much more uniform through its thickness, both in terms of the pore size and the plaque porosity. It still exhibits the more dense "skin" that is generally associated with slurry plaque; however, the reduced porosity in this "skin" region is less pronounced. One sample (6A) displayed a peak to 40 μm in the pore size that corresponded to some small voids about 60–70% through the thickness of this piece. The plaque porosity in is quite uniform through the thickness, except near the center where the substrate grid causes a pronounced drop in porosity. As shown in Figure 23, the location of this grid can vary significantly within the plaque over different samples of plaque.

The plaque samples from the aqueous slurry process included samples of three differing thicknesses and two differing average porosities, yet no real systematic variations in either pore size or plaque porosity are seen in response to these process changes (except the expected 2% higher porosity for the 78% porous plaque samples). This apparent insensitivity of the pore characteristics to intentional process changes suggests that the process controls are relatively robust for making this type of plaque.

5.3 Dry-Powder Sintered Plaque

As indicated in Table 1, eight samples of dry-powder plaque were analyzed. The typical variation in pore size distribution through the thickness of these samples is shown in Figure 24. In this figure the pores on the screen side of the plaque consist of two overlapping distributions. A sub-distribution peaking at about 30 μm appears to correspond to a uniform distribution that exists in the sinter that is not in the vicinity of the grid wires. The sinter on the screen side of the dry powder plaque always appears to be slightly denser than that on the other side, a consequence of preferential packing of the

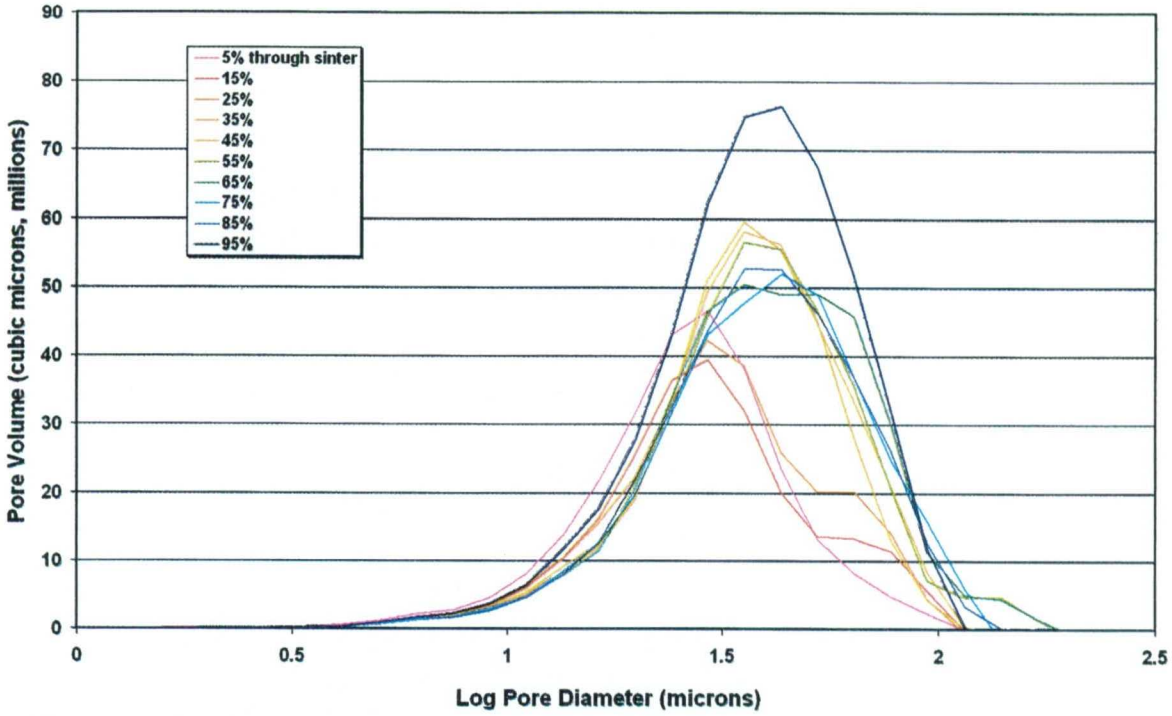

Figure 24. Changes in the pore size distribution through the thickness of a typical sample of dry-powder plaque. These data are from sample 4A.

dry powder prior to sintering. The second sub-distribution on the screen side of the plaque, which peaks at about 60 μm, appears to coincide with larger pores in the sinter that occur around the grid wires, and which are illustrated in Figure 8. As one moves away from the screen side of the dry-powder plaque, the distribution of pores transitions into a single, relatively wide distribution that peaks around 40 μm, and is wide enough to encompass the full width of the distributions seen on the more dense side of the plaque.

The changes in the pore size distributions are more easily compared for the different plaque samples by plotting the average pore size and the average sinter porosity as a function of the plaque thickness. These plots are shown in Figures 25 through 28 for the dry-powder plaque samples in Groups 4 and 5.

The pore sizes for the dry-powder plaque range from 30 to 50 μm through the thickness of the samples, with a pronounced gradient favoring larger pores on the side away from the screen. These pore sizes are generally larger than for the regions in slurry plaque that do not contain large voids, whether alcohol or water based. Because the dry-powder plaque has its internal nickel-supporting screen on one side, the plaque has intrinsic gradients through its thickness. The screen side can have a somewhat denser plaque because the nickel powder settles slightly before it is sintered and because of the dense screen wires. However, this effect can be offset by voids that can form around the grid wires. These effects combine to produce the characteristic porosity profiles seen in Figures 26 and 28 for dry powder plaque.

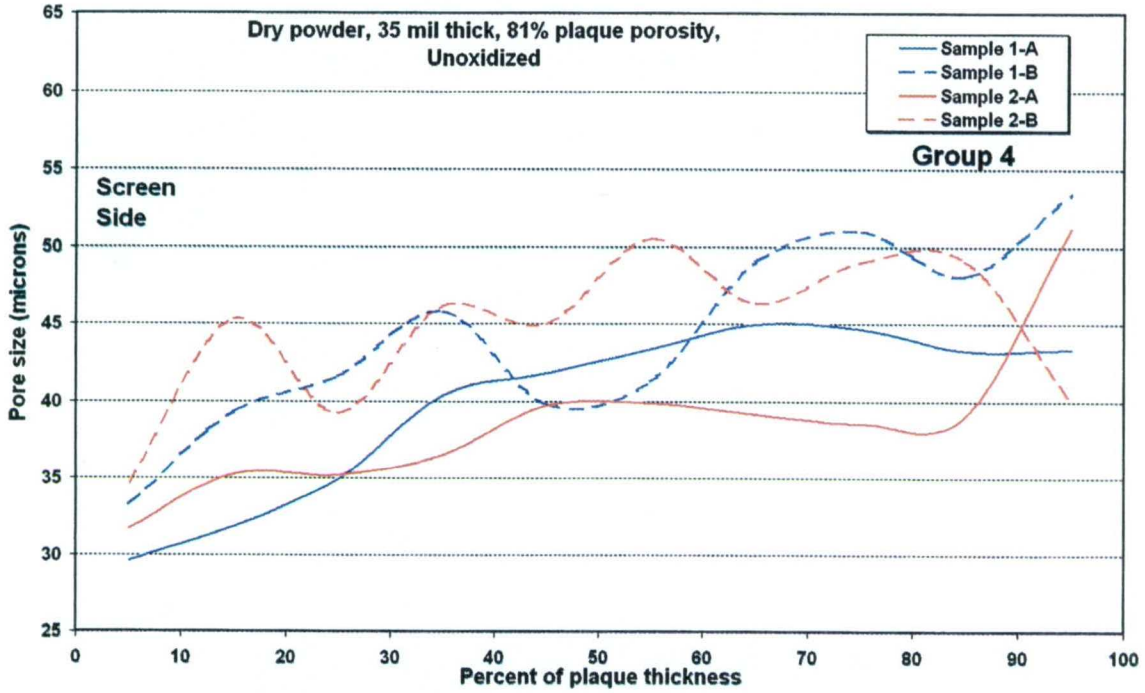

Figure 25. Variation in the average pore size through the thickness of dry-powder plaque samples from Group 4.

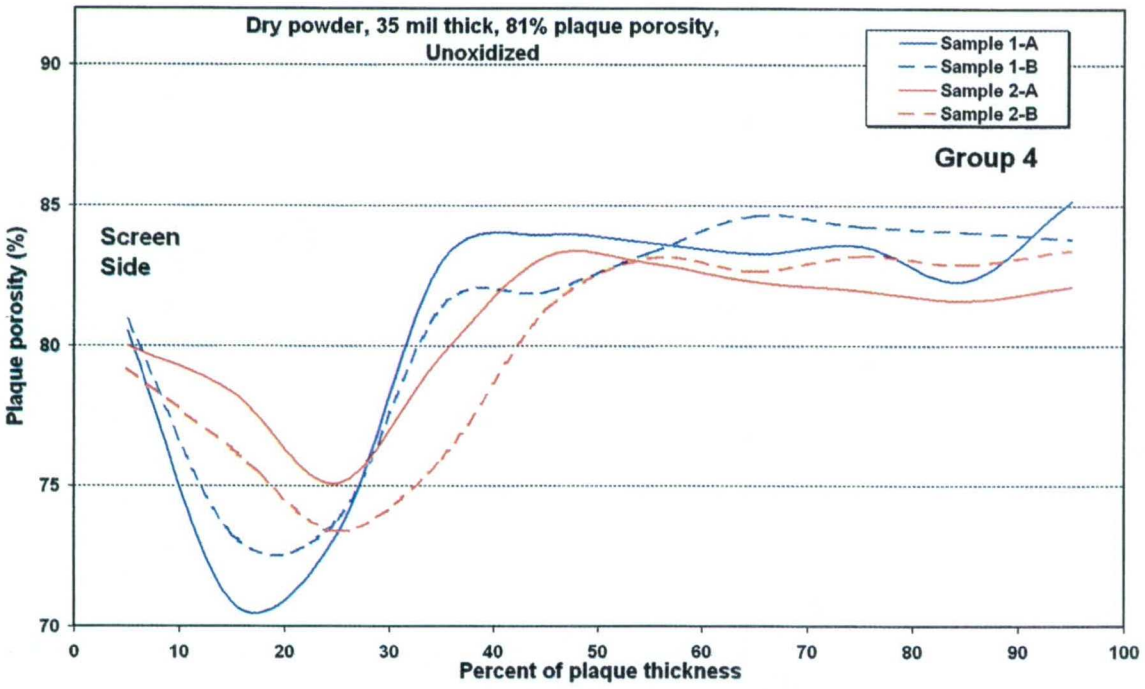

Figure 26. Variation in the average plaque porosity through the thickness of dry-powder plaque samples from Group 4. The overall plaque porosity in these samples is nominally 84%.

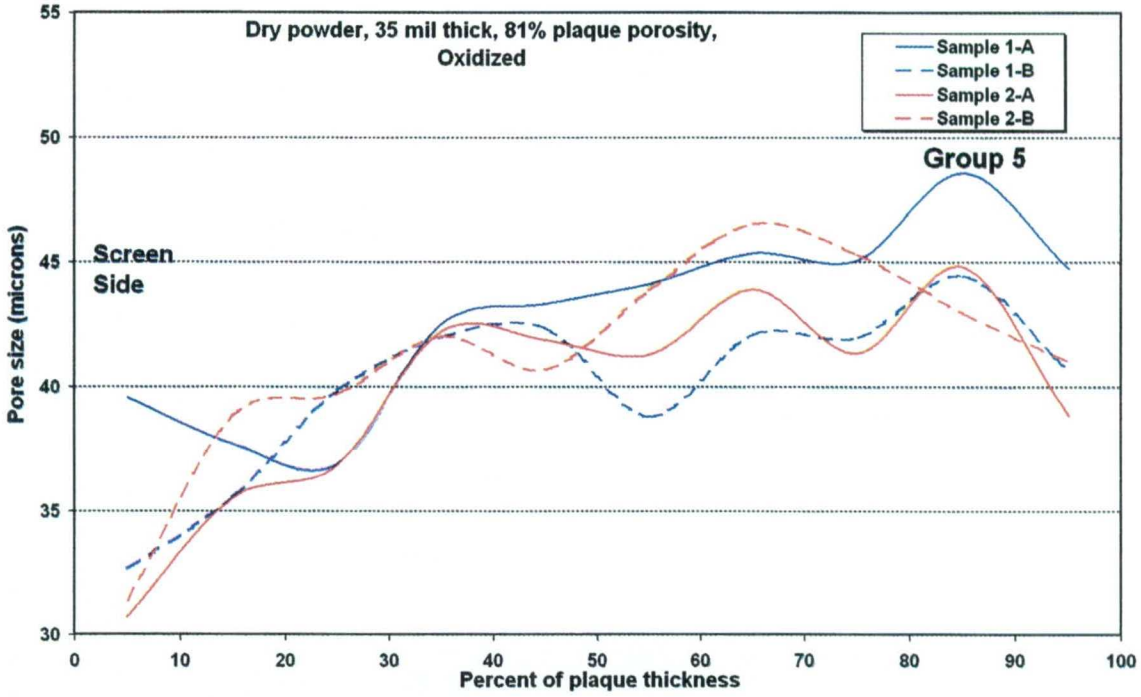

Figure 27. Variation in the average pore size through the thickness of dry-powder plaque samples from Group 5.

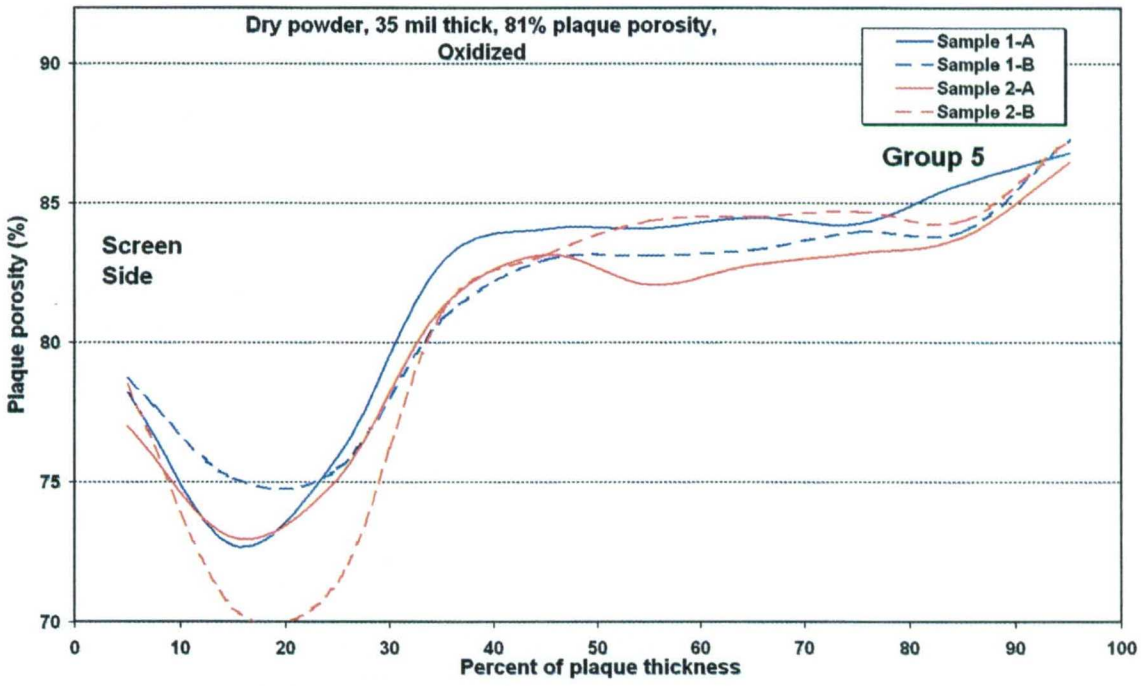

Figure 28. Variation in the average plaque porosity through the thickness of dry-powder plaque samples from Group 5. The overall plaque porosity in these samples is nominally 84%.

While the pore sizes within dry-powder plaque are seen to vary in the 30–50 μm range, there is not an extremely large variation in the average plaque porosity except for the pronounced drop resulting from the dense screen wires near the screen side of the plaque. The densest "skin" at the screen side of the dry-powder plaque drops to 77–80% porosity, which is 4–7% lower than the nominal overall sinter porosity of about 84% (the average sinter porosity is about 4% higher than the average plaque porosity). On the side away from the screen, the porosity at the plaque surface is about 84–87%, which is less than 3% higher than the average porosity expected for the sinter in this type of plaque.

Similarly, the interior regions of the dry-powder plaque remain consistently in the 82–85% porosity range, which is within about 2% of the nominal average sinter porosity expected in dry-powder plaque. This interior sinter porosity is even closer to the average if it is noted (by examination of Table 1) that most of these dry-powder plaque samples had an overall plaque porosity about 1% greater than the nominal 80% porosity expected for this type of dry-powder plaque. Thus, the sinter (excluding the effects of the screen wires) in these dry-powder plaque samples appears to range from about 78% porosity in a skin on the screen side to a relatively uniform 84% porosity in the interior, and finally a less dense region on the topside having a porosity of about 86–87%.

6. Discussion of Results

Each of the three types of sintered plaque analyzed here displays some unique signatures in terms of the pore size distributions, as well as their uniformity through the thickness and over the surface of the plaque samples. The average pore sizes are compared in Figure 29 for the different types of plaque samples. Average pore sizes are generally expected to increase as the overall plaque porosity increases, as is suggested by the results in Figure 29 for groups 4–6. However, the alcohol-based slurry plaque displays a large variability in average pore size, ranging from 32.1 μm for group 3 to 40.3 μm in group 1. Most of this variability results from the variable incidence of large voids in this type of plaque. While the dry-powder plaque displayed relatively large average pore sizes, many of the larger pores occurred around the grid wires in this design and appear to be a consistent feature of the dry-powder plaque fabrication process.

The alcohol-based slurry plaque displays pore distributions that are dominated by large internal voids combined with regions of highly densified sinter. These highly non-uniform regions of sinter occur in more than 50% of the plaque samples analyzed; however, a number of regions containing much more uniform distributions of pore sizes were also observed. Similarly, the dry-powder plaque, while quite uniform through much of its thickness, displayed frequent large voids around the screen wires. Thus, the pore characteristics of the alcohol-based slurry plaque and the other types of plaque studied here are probably best evaluated based on the uniformity of the pore distribution through the plaque thickness from sample to sample.

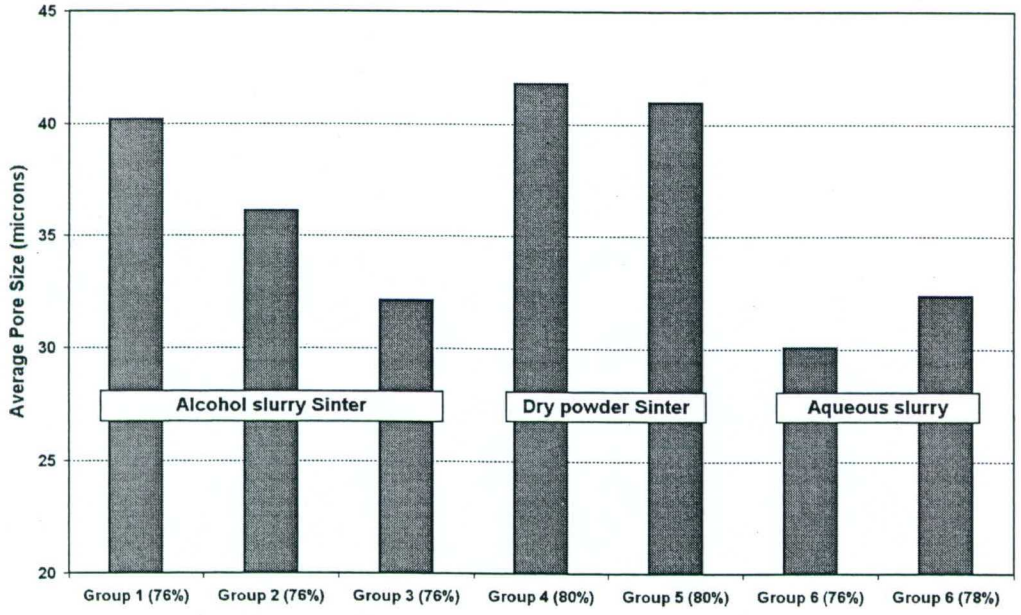

Figure 29. Variation of the average pore size (at 50% cumulative pore volume) for the different groups of plaque samples studied here.

Evaluation of pore uniformity was based on the range of observed pore sizes or porosity through the thickness of all samples from each plaque group as a percentage of the overall average pore size or porosity. Pore variability or uniformity expressed in this manner is indicated in Figures 30 and 31. Figure 30 graphically shows that pore size uniformity is poor and highly variable in the alcohol-based slurry, while the dry-powder plaque and water-based slurry plaque have considerably less pore size variability.

Figure 31 shows the variation in the porosity through the ten bins that cover the thickness of the plaque samples in each of the groups studied. Thus, zero porosity variability would correspond to identical porosity in all ten bins for all the samples in each group. The porosity variability of 25.8–35.8% for the alcohol-based slurry is similar, but slightly greater than the 15.8–33.7% variability seen for the water-based slurry plaque. The dry-powder plaque is the most uniform in terms of variations in porosity, with a range of 17.8–20.7%.

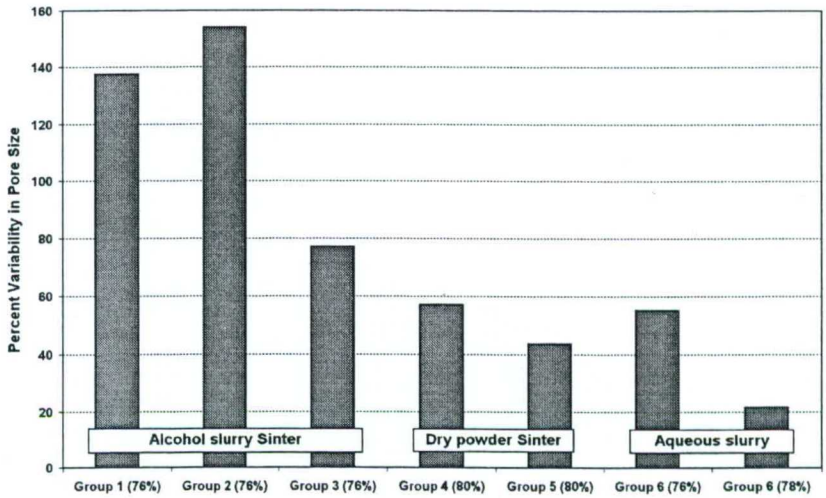

Figure 30. Variability in pore size (as a percentage of overall average pore size) for each type of plaque.

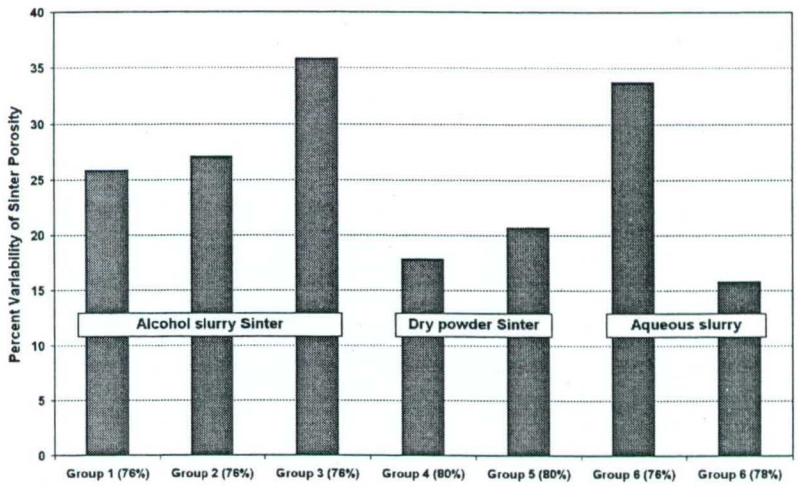

Figure 31. Variability in plaque porosity (as a percentage of overall average sinter porosity) for each type of plaque.

7. Conclusions

The porosity characteristics of sintered nickel plaque made by three different processes has been evaluated by a new analysis method that locates the pores in SEM images. Some significant differences in the internal structure of these different types of plaque have been observed. The structure of the alcohol-based slurry plaque tends to contain large internal voids as well as high-density aggregates of nickel that make the plaque porosity and pore sizes highly non-uniform. This type of nonuniformity was seen through the thickness of the alcohol-based slurry plaque, and was also found to be highly variable from one area of plaque to another.

The dry-powder plaque and the water-based slurry plaque were both found to be much more uniform, in spite of having very different average internal pore sizes. The aqueous slurry plaque (and the uniform regions of the alcohol-based slurry plaque) displayed a smaller average pore size than did the dry-powder plaque. The aqueous slurry plaque production process appears to offer a means to consistently obtain the smaller average pore sizes associated with the slurry process, along with the high degree of pore uniformity associated with the dry-powder process.

References

. 1 Zimmerman, A. H. and G. A. To, "Porosity Characteristics of Nickel Sinter," TR-2005(8555)-1, The Aerospace Corporation, 15 February 2005.

2. Zimmerman, A. H., G. A. To and M. V. Quinzio, "Scanning Porosimetry for Characterization of Porous Electrode Structures," *Proc. of the 17th Annual Battery Conf. on Appl. and Adv.*, IEEE 02TH8576, ISBN 0-7803-7132-1, 2002, pp. 293-298.

LABORATORY OPERATIONS

The Aerospace Corporation functions as an "architect-engineer" for national security programs, specializing in advanced military space systems. The Corporation's Laboratory Operations supports the effective and timely development and operation of national security systems through scientific research and the application of advanced technology. Vital to the success of the Corporation is the technical staff's wide-ranging expertise and its ability to stay abreast of new technological developments and program support issues associated with rapidly evolving space systems. Contributing capabilities are provided by these individual organizations:

Electronics and Photonics Laboratory: Microelectronics, VLSI reliability, failure analysis, solid-state device physics, compound semiconductors, radiation effects, infrared and CCD detector devices, data storage and display technologies; lasers and electro-optics, solid-state laser design, micro-optics, optical communications, and fiber-optic sensors; atomic frequency standards, applied laser spectroscopy, laser chemistry, atmospheric propagation and beam control, LIDAR/LADAR remote sensing; solar cell and array testing and evaluation, battery electrochemistry, battery testing and evaluation.

Space Materials Laboratory: Evaluation and characterizations of new materials and processing techniques: metals, alloys, ceramics, polymers, thin films, and composites; development of advanced deposition processes; nondestructive evaluation, component failure analysis and reliability; structural mechanics, fracture mechanics, and stress corrosion; analysis and evaluation of materials at cryogenic and elevated temperatures; launch vehicle fluid mechanics, heat transfer and flight dynamics; aerothermodynamics; chemical and electric propulsion; environmental chemistry; combustion processes; space environment effects on materials, hardening and vulnerability assessment; contamination, thermal and structural control; lubrication and surface phenomena. Microelectromechanical systems (MEMS) for space applications; laser micromachining; laser-surface physical and chemical interactions; micropropulsion; micro- and nanosatellite mission analysis; intelligent microinstruments for monitoring space and launch system environments.

Space Science Applications Laboratory: Magnetospheric, auroral and cosmic-ray physics, wave-particle interactions, magnetospheric plasma waves; atmospheric and ionospheric physics, density and composition of the upper atmosphere, remote sensing using atmospheric radiation; solar physics, infrared astronomy, infrared signature analysis; infrared surveillance, imaging and remote sensing; multispectral and hyperspectral sensor development; data analysis and algorithm development; applications of multispectral and hyperspectral imagery to defense, civil space, commercial, and environmental missions; effects of solar activity, magnetic storms and nuclear explosions on the Earth's atmosphere, ionosphere and magnetosphere; effects of electromagnetic and particulate radiations on space systems; space instrumentation, design, fabrication and test; environmental chemistry, trace detection; atmospheric chemical reactions, atmospheric optics, light scattering, state-specific chemical reactions, and radiative signatures of missile plumes.